AGU PUBLICATIONS

JGR

Journal of Geophysical Research: Solid Earth

RESEARCH ARTICLE
10.1002/2013JB010724

Key Points:
- Trapped waves in fault zones modulate the kinematic properties of ruptures
- Relations between fault-zone structure and rupture properties are characterized
- Fault zone waves enable rupture at speeds unstable in homogeneous media

Supporting Information:
- Readme
- Text S1
- Figure S1

Correspondence to:
Y. Huang,
yihe@gps.caltech.edu

Citation:
Huang, Y., J.-P. Ampuero, and D. V. Helmberger (2014), Earthquake ruptures modulated by waves in damaged fault zones, *J. Geophys. Res. Solid Earth*, *119*, 3133–3154, doi:10.1002/2013JB010724.

Received 26 SEP 2013
Accepted 26 MAR 2014
Accepted article online 30 MAR 2014
Published online 11 APR 2014

Earthquake ruptures modulated by waves in damaged fault zones

Yihe Huang[1], Jean-Paul Ampuero[1], and Don V. Helmberger[1]

[1]Division of Geological and Planetary Sciences, California Institute of Technology, Pasadena, California, USA

Abstract Faults are usually surrounded by damaged zones of lower elastic moduli and seismic wave velocities than their host rocks. If the interface between the damaged rocks and host rocks is sharp enough, earthquakes happening inside the fault zone generate reflected waves and head waves, which can interact with earthquake ruptures and modulate rupture properties such as rupture speed, slip rate, and rise time. We find through 2–D dynamic rupture simulations the following: (1) Reflected waves can induce multiple slip pulses. The rise time of the primary pulse is controlled by fault zone properties, rather than by frictional properties. (2) Head waves can cause oscillations of rupture speed and, in a certain range of fault zone widths, a permanent transition to supershear rupture with speeds that would be unstable in homogeneous media. (3) Large attenuation smears the slip rate function and delays the initial acceleration of rupture speed but does not affect significantly the rise time or the period of rupture speed oscillations. (4) Fault zones cause a rotation of the background stress field and can induce plastic deformations on both extensional and compressional sides of the fault. The plastic deformations are accumulated both inside and outside the fault zone, which indicates a correlation between fault zone development and repeating ruptures. Spatially periodic patterns of plastic deformations are formed due to oscillating rupture speed, which may leave a permanent signature in the geological record. Our results indicate that damaged fault zones with sharp boundaries promote multiple slip pulses and supershear ruptures.

1. Introduction

The kinematics of earthquake ruptures can be represented by three key parameters: slip rate, rise time (the duration of slip at a given point), and rupture speed. Seismic observations suggest that these parameters are highly variable. Rise time can either be comparable to the overall duration of the event as suggested by crack model [*Madariaga*, 1976] or much shorter than the overall duration, which leads to the so-called slip pulse model [*Heaton*, 1990]. Several mechanisms have been proposed to explain the generation of slip pulses, including self-healing due to velocity-dependent friction [*Perrin et al*., 1995; *Beeler and Tullis*, 1996] and healing fronts induced by stress heterogeneities [*Day*, 1982; *Beroza and Mikumo*, 1996]. Ruptures can also become supershear, i.e., reach a speed faster than the shear wave speed, as observed in the 1979 Imperial Valley earthquake [*Archuleta*, 1984; *Spudich and Cranswick*, 1984], the 1999 Izmit earthquake [*Bouchon et al*., 2001, 2002], the 2001 Kunlunshan earthquake [*Bouchon and Vallee*, 2003; *Walker and Shearer*, 2009], and the 2002 Denali earthquake [*Dunham and Archuleta*, 2004; *Ellsworth et al*., 2004; *Walker and Shearer*, 2009]. Theoretical and laboratory models of supershear ruptures require the shear stress on the fault to be close enough to the static frictional strength, relative to the stress drop [*Andrews*, 1976; *Xia et al*., 2004; *Dunham*, 2007].

Current models of slip pulses and supershear ruptures have been developed under the simplifying assumption of a uniform elastic medium or a bimaterial interface. However, faults are often surrounded by damaged fault zones [*Chester and Logan*, 1986; *Sibson*, 1986; *Scholz*, 1987; *Chester and Chester*, 1998; *Ben-Zion and Sammis*, 2003; *Savage and Brodsky*, 2011; *Rowe et al*., 2013] caused by either aseismic deformation [*Cowie and Scholz*, 1992; *Chester and Chester*, 2000; *Childs et al*., 2009; *Faulkner et al*., 2011] or by coseismic processes [*Rice et al*., 2005; *Ben-Zion and Ampuero*, 2009; *Sagy and Korngreen*, 2012; *Xu et al*., 2012; *Rempe et al*., 2013; *Johri et al*., 2014]. A typical manifestation of damage is a reduced seismic wave velocity (Table 1). Due to the significant velocity reductions inside fault zones, these structures can trap seismic waves that can continuously perturb stresses on the fault during earthquakes. Previous numerical modeling of dynamic ruptures inside fault zones, assuming ideal elastic media, indicates that these low-velocity structures can cause the generation of slip pulses and accelerate the transition to supershear rupture [*Harris and Day*, 1997;

Table 1. Summary of Material Properties of Main Fault Zones

Fault Zones	Width (m)	Velocity Reduction (%)	Q_s	References
San Andreas	~ 150	30–40	10–40	*Lewis and Ben-Zion* [2010]
	~ 200			*Li et al.* [2006]
San Jacinto	125–180	35–45	20–40	*Lewis et al.* [2005]
	150–200	25–60		*Yang and Zhu* [2010]
Landers	270–360	35–60		*Li et al.* [2007]
	150–200	30–40	20–30	*Peng et al.* [2003]
Hector Mine	75–100	40–50	10–60	*Li et al.* [2002]
Calico	~ 1500	40–50		*Cochran et al.* [2009]
	~ 1300	40–50		*Yang et al.* [2011]
Nojima	100–220			*Mizuno et al.* [2008]
Anatolian	~ 100	50	10–15	*Ben-Zion et al.* [2003]

Huang and Ampuero, 2011], which otherwise do not exist in a uniform medium given the same initial conditions and friction parameters. These results suggest that in the regions where damaged fault zones are observed (Table 1), earthquake ruptures can have complexities such as short rise time and supershear rupture speed due to the influence of fault zones.

Previous findings also pose several new questions: Which waves cause the generation of slip pulses and the rapid transition to supershear rupture? Can these waves exist in fault zones despite large attenuation and off-fault plasticity? What are the differences between slip pulses and supershear ruptures induced by fault zone waves and those generated by other mechanisms? In this paper, we aim to answer these questions through dynamic rupture modeling. We focus on fault zones bounded by sharp material interfaces, as an end-member class of fault zone structures in which the phenomena described are exacerbated. We describe our model assumptions and methods in section 2. In section 3, based on dynamic rupture simulations on faults in a homogeneous medium and in fault zones, we show how the velocity reduction and width of elastic fault zones affect the slip rate, rise time, and rupture speed. In section 4, by comparing the results of dynamic rupture simulations with the stress wavefield induced by a point source, we identify the waves that cause variations of rise time and rupture speed in fault zones. The effects of inelasticity within the fault zone are examined in section 5. Implications for earthquake ruptures in natural fault zones are discussed in section 6.

2. Model Description

We consider a 2-D inplane rupture on a planar fault that bisects a fault zone (Figure 1). The fault zone is embedded in an infinite medium composed of a host rock. We define the width of the fault zone as W^{FZ} and the relative velocity reduction as $\Delta v = 1 - v^{FZ}/v^{host}$ (%), where v^{FZ} and v^{host} are wave speeds inside the fault zone and host rock, respectively. Subscripts "*p*" and "*s*" denote *P* and *S* waves. For example, v_s^{host} denotes the *S* wave speed in the host rock. We assume that Δv is the same for *P* and *S* waves unless otherwise specified.

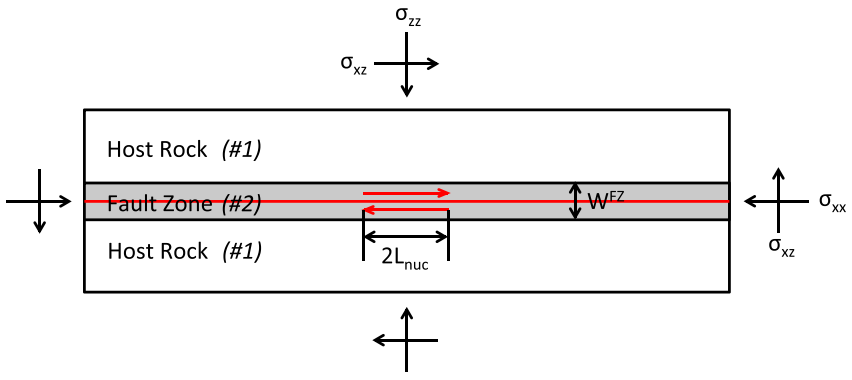

Figure 1. Model setup of the 2-D inplane rupture on a fault that bisections a fault zone embedded in a host rock. The host rock and fault zone are composed of material #1 and #2, respectively. The rupture is nucleated by an overstressed patch in the middle, which has a width 2 L_{nuc}.

We adopt a strongly velocity weakening friction law, which reproduces the dramatic weakening of friction at seismic slip rates ($>$ 0.1 m/s) observed in high-speed rock experiments [*Reches and Lockner*, 2010; *Goldsby and Tullis*, 2011]. The friction law agrees with laboratory data in that the steady state friction drop is proportional to $1/v$ when the slip rate, v, is larger than a critical velocity scale v_c. This feature is also predicted by theoretical models of weakening by flash heating [*Rice*, 2006; *Beeler et al.*, 2008]. The sliding friction μ_f and the evolution of a state variable θ are controlled by the static friction coefficient μ_s, the critical slip distance D_c, the characteristic velocity scale v_c, and the two positive coefficients α and β [*Ampuero and Ben-Zion*, 2008; *Gabriel et al.*, 2012]:

$$\mu_f = \mu_s + \alpha \frac{v}{v + v_c} - \beta \frac{\theta}{\theta + D_c} \tag{1}$$

$$\frac{\mathrm{d}\theta}{\mathrm{d}t} = v - \frac{v_c \theta}{D_c} \tag{2}$$

The value of v_c is in the range of 0.05 to 2 m/s based on theoretical models [*Beeler et al.*, 2008], while *Goldsby and Tullis* [2011] suggest a value of ~ 0.1 m/s from laboratory experiments. The dynamic friction coefficient μ_d is defined as the steady state sliding friction at infinitely high slip velocity: $\mu_d = \mu_s + \alpha - \beta$. The state evolution equation (2) encapsulates two physical ingredients: slip weakening and time-dependent healing. The state variable relaxes exponentially toward its steady state value, $\theta = vD_c/v_c$, over a characteristic time scale D_c/v_c. In the limit of fast sliding well above steady state, $v \gg \theta v_c/D_c$, the state is proportional to slip and the evolution effect of the friction law (the last term in equation (1)) yields slip weakening with characteristic slip scale D_c. At very low sliding speed well below steady state, $v \ll \theta v_c/D_c$ and the friction evolution is dominated by exponential time-dependent healing.

Due to the symmetry of the problems considered here, the normal stress σ_0 remains constant. We assume a spatially uniform normal stress. We artificially start ruptures by setting an overstressed nucleation patch of width 2 L_{nuc} around the hypocenter. Inside the nucleation patch, the initial shear stress τ_0 is slightly above the static strength $\tau_y = \sigma_0 \mu_s$. Outside the nucleation patch, τ_0 is chosen uniform and small enough to ensure subshear rupture in a homogeneous medium but large enough to nucleate rupture successfully by using a nucleation patch of reasonable size. Specifically, we set the nominal relative strength parameter [*Das and Aki*, 1977] as $S = (\tau_y - \tau_0)/(\tau_0 - \tau_d) = 1.7$, where $\tau_d = \sigma_0 \mu_d$ is the steady state dynamic strength at very high slip rate. We will discuss the influence of different τ_0 in section 6. Given a certain v_c, a transition from dying ruptures to sustained ruptures occurs as L_{nuc} is increased in a homogeneous medium [*Ampuero and Ben-Zion*, 2008]. In our simulations we set the value of L_{nuc} large enough to get sustained ruptures for the range of v_c we considered.

We solve the problem of dynamic rupture in fault zones numerically with a 2-D spectral element method (SEM2DPACK, http://www.sourceforge.net/projects/sem2d/). The numerical method is described (in 3-D) by *Kaneko et al.* [2008] and has been applied in previous work [e.g., *Madariaga et al.*, 2006; *Kaneko et al.*, 2011; *Huang and Ampuero*, 2011; *Gabriel et al.*, 2012, 2013; *Xu et al.*, 2012]. The element size is set small enough to ensure well-resolved results based on a priori criteria described by *Ampuero and Ben-Zion* [2008] and on a posteriori verification that the process zone is resolved by more than five grid nodes. Numerical convergence as a function of element size is demonstrated in the supporting information.

3. Ruptures in Elastic Fault Zones

3.1. Dimensionless Quantities and Reference Simulation in Homogeneous Media

We show the results of dynamic rupture models in elastic media in this section. We first illustrate, for reference, the behavior of ruptures in the absence of fault zones. We then show the changes of rupture behavior induced by fault zones with different widths and velocity reductions. To preserve the generality of the problem, we use dimensionless quantities for space x, time t, slip D, slip velocity D', and stress τ throughout section 3:

$$\widetilde{x} = x/L_c \tag{3}$$

$$\widetilde{t} = t v_s^{\mathrm{host}}/L_c \tag{4}$$

$$\widetilde{D} = D/D_c \tag{5}$$

$$\widetilde{D'} = D'/v_{\mathrm{dyn}} \tag{6}$$

$$\widetilde{\tau} = \tau/\Delta\tau_s \tag{7}$$

Table 2. Dimensionless Model Parameters

Parameter	Description	Value
ρ	Density	1
v_p^{host}	P wave speed in the host rock	1.732
v_s^{host}	S wave speed in the host rock	1
σ_0	Normal stress	2
τ_0	Initial shear stress	0.57
μ_s	Static friction coefficient	0.6
D_c	Critical slip distance	1
v_c	Characteristic velocity scale	0.04/0.1
α	Direct effect coefficient	0.005
β	Evolution effect coefficient	0.505

Given shear modulus G^{host}, we define the following parameters:

$$L_c = G^{host} D_c / \Delta\tau_s \quad (8)$$

$$v_{dyn} = v_s^{host} D_c / L_c \quad (9)$$

$$\Delta\tau_s = (\mu_s - \mu_d)\sigma_0 = \tau_y - \tau_d \quad (10)$$

Our results can be applied to a variety of initial conditions by converting these dimensionless quantities. For example, when $G^{host} = 30$ GPa and $\Delta\tau_s = 30$ MPa, we find $L_c = 100$ m for $D_c = 0.1$ m and $L_c = 1$ km for $D_c = 1$ m. The values of dimensionless parameters are summarized in Table 2. Among them, α needs to be a small but positive number to avoid ill-posedness, while β is given by the equation $\mu_d = \mu_s + \alpha - \beta$.

In a homogeneous medium, rupture behavior is controlled by friction parameters and initial stresses on the fault. Especially, increasing the critical velocity scale v_c induces a transition from crack-like rupture to pulse-like rupture (Figure 2). At a certain value of v_c (which depends on the initial stress), the rise time becomes shorter than the total rupture time and then decreases with increasing v_c [*Ampuero and Ben-Zion*, 2008]. The characteristic time scale D_c/v_c in the strong-velocity weakening friction law (equation (2)) controls the time scale for frictional strength to increase and hence the emergence of healing fronts and the crack-to-pulse transition. For small values of v_c (Figure 2a), the friction law functions more like slip weakening [*Shaw and Rice*, 2000; *Ampuero and Ben-Zion*, 2008], and the rupture propagates as a crack. A large v_c (Figure 2b) favors pulse-like ruptures and shorter rise time.

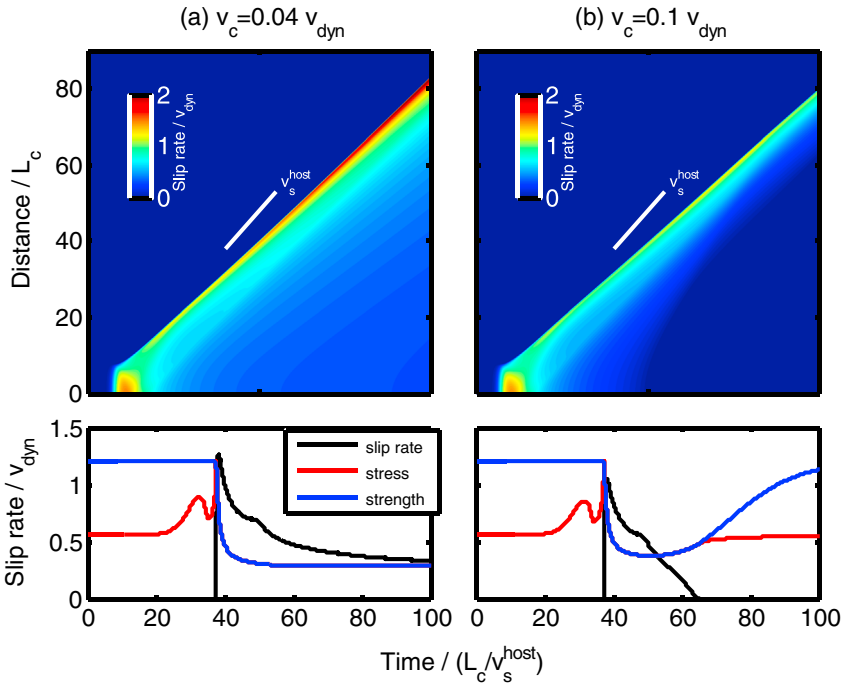

Figure 2. (top) Spatiotemporal view of slip rate and (bottom) slip rate, stress, and frictional strength at a distance of 30 L_c from the hypocenter for ruptures in a homogeneous medium with two different values of the characteristic velocity of frictional weakening, v_c. The white solid lines in Figures 2a and 2b denote v_s^{host}. Rupture speed v_r^{host} is about 0.8 v_s^{host}.

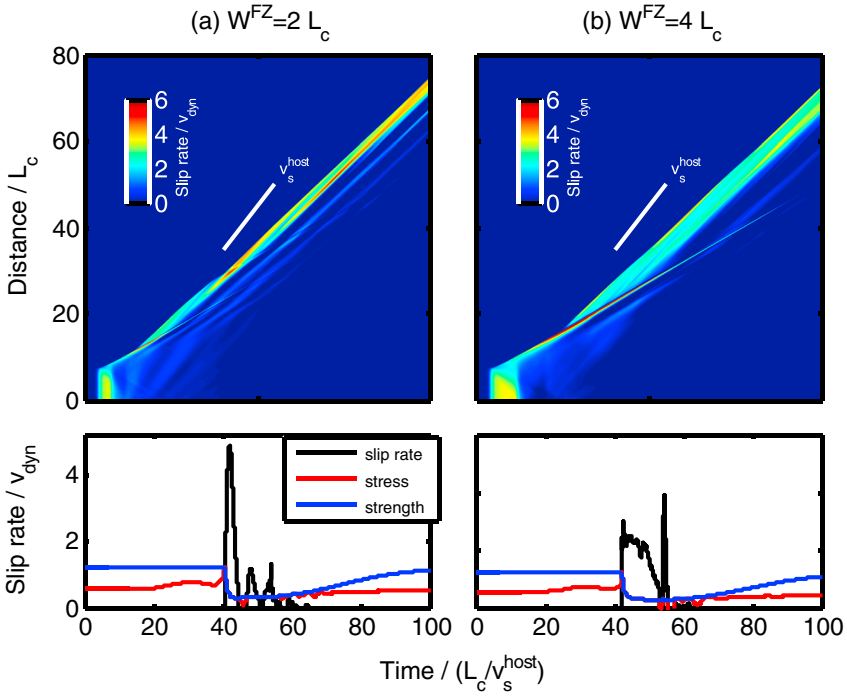

Figure 3. (top) Spatiotemporal view of slip rate and (bottom) slip rate, stress, and frictional strength at a distance of 30 L_c of ruptures in fault zones of 50% velocity reduction with two different fault zone widths ($v_c = 0.1\ v_{dyn}$). The white solid lines in Figures 3a and 3b denote v_s^{host}.

3.2. Multiple Pulses and Rise Times

In the presence of fault zones, a second characteristic time scale, W^{FZ}/v^{FZ}, is provided by the waves reflected at the interfaces bounding the fault zone. Waves with precritical incidence angles continuously leak energy out of the fault zone, while waves with postcritical incidence angles are trapped inside due to total reflections. Constructively interfering trapped waves can modulate stresses on the fault and strongly affect ruptures, especially if they reach the rupture front. We refer to all these waves inside fault zones as *fault zone waves*. These waves will be described in detail in section 4. In summary, ruptures in fault zones with strongly velocity weakening friction are controlled by two characteristic time scales: the time scale of wave propagation W^{FZ}/v^{FZ} and the time scale of frictional healing D_c/v_c. Next we will show results of dynamic rupture simulations under fixed friction parameters ($D_c = 1$ and $v_c = 0.1\ v_{dyn}$, as in the homogeneous example shown in Figure 2b) but varying the time scale of wave propagation.

We have shown before that fault zones can induce slip pulses and control their rise time [*Huang and Ampuero*, 2011]. The same effects of fault zones appear in our current study, but our new simulations allow for a deeper insight into the rich range of phenomena and their underlying mechanisms. We first consider ruptures in fault zones of 50% velocity reduction (Δv = 50%) for W^{FZ}/L_c = 2 and 4. When W^{FZ} = 2 L_c, we find that slip rate is highly oscillatory compared to ruptures in a homogeneous medium, leading to multiple short pulses (Figure 3a). Depending on their polarity, fault zone reflected waves induce fault stress perturbation that may be favorable or unfavorable for slip. Slip stops upon the arrival of each fault zone reflected wave that carries an unfavorable stress perturbation and may resume multiple times when each reflected wave with favorable stress arrives. The rise time of the first pulse is near 5.5 L_c/v_s on average, almost one fourth of that in a homogeneous medium (Figure 2b). When W^{FZ} = 4 L_c, the rupture evolves into a large pulse with sharp healing front, followed by shorter pulses (Figure 3b). The rise time of the first large pulse is about 11 L_c/v_s on average, still shorter than in a homogeneous medium but twice longer than in the case of W^{FZ} = 2 L_c. As we will show later in section 4, the rise time of the first pulse is controlled by reflected waves in fault zones and thus proportional to W^{FZ}. Peak slip rate is larger than that in the homogeneous case by more than a factor of 2. Note that in both cases the total rise time, defined as the time between the onset of the first pulse and the end of the last pulse, is still determined by self-healing caused by strongly velocity weakening friction. Since it

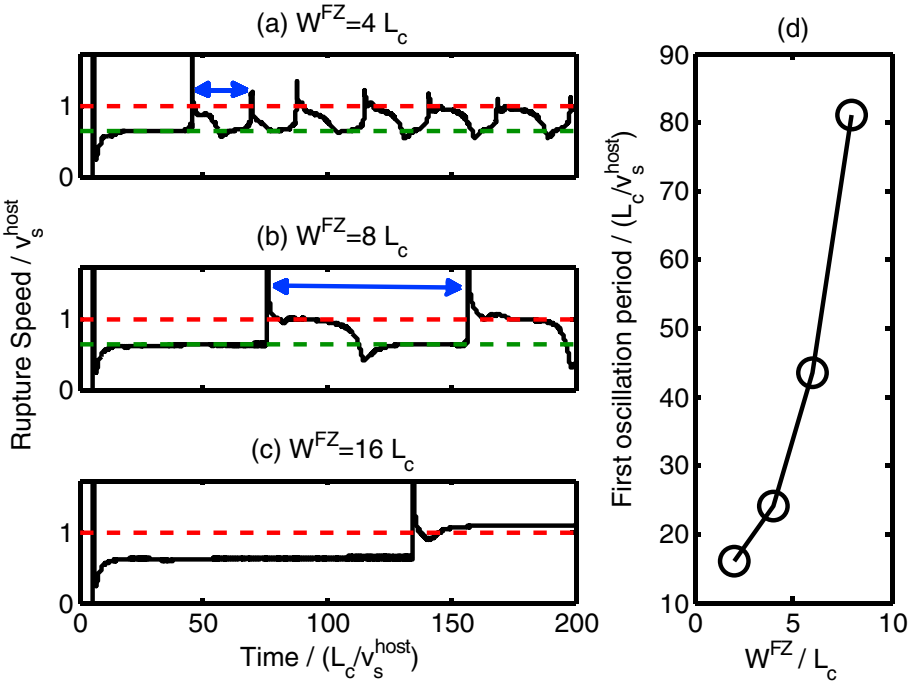

Figure 4. (a–c) Rupture speed as a function of time in fault zones of 30% velocity reduction with three different fault zone widths. We calculate rupture speeds based on the position and timing of the tail of the process zone (defined as the location where slip equals D_c) to avoid ad hoc smoothing. Rupture front in a fault zone of 30% velocity reduction with a fault zone width of 4 L_c is shown in Figures 10 and 11. Red dashed lines denote v_s^{host} and green dashed lines denote Rayleigh wave speed of the fault zone. Blue arrows mark the first rupture speed oscillation period. (d) Period of the first rupture speed oscillation in fault zones of 30% velocity reductions as a function of fault zone width.

is hard to accurately measure the total rise time from observations, for practical purpose we only consider the rise time of the first pulse, which accomplishes more than 80% of the final slip in both cases after ruptures reach steady state. The above examples show that both rise time and slip rate of the first pulse are controlled by the structural and material properties of the fault zone, rather than by the friction parameters.

3.3. Oscillatory Rupture Speeds and Enhanced Supershear Transition

In a homogeneous medium, rupture approaches a speed $v_r^{host} \approx 0.8\, v_s^{host}$ quickly after the nucleation (Figure 2). The value of v_r^{host} depends primarily on the state of stresses (the S ratio) as discussed by *Gabriel et al.* [2012]. In the fault zones with Δv = 50%, rupture speed approaches v_r^{host} for both values of W^{FZ} (Figure 3), but if Δv = 30% rupture speed oscillates strongly instead (Figure 4). Rupture speed is calculated based on the position and timing of the tail of the process zone (defined as the location where slip equals D_c) to achieve stable estimates without ad hoc smoothing. The oscillations of rupture speed become more pronounced as W^{FZ} increases (compare the differences between maximum and minimum rupture speeds in Figures 4a and 4b). When W^{FZ} = 4 L_c and 8 L_c, rupture speed oscillates between a minimum value slower than the Rayleigh wave speed of the fault zone material and a maximum value faster than v_s^{host}. Because of accelerations and decelerations of the rupture front, the rise time of the first pulse also oscillates, but the average rise time is still short compared to the total rupture time. The period of the first rupture speed oscillation (denoted by blue arrows in Figures 4a and 4b) increases as a function of fault zone width, W^{FZ}, and apparently diverges at a finite value $W^{FZ}/L_c \approx 10$ (Figure 4d).

For the case with W^{FZ} = 16 L_c (Figure 4c), the rupture jumps to a speed faster than v_s^{host} and then remains at a speed near v_p^{FZ}. Note that the rupture is supershear relative to both the host rock and fault zone. This supershear rupture speed persists for much longer time than shown in Figure 4c. The disappearance of rupture oscillations at large fault zone widths (Figure 4d) also indicates that the supershear transition is permanent. Given the assumed initial stresses, supershear ruptures do not exist in a homogeneous medium with the material properties of the host rock [*Gabriel et al.*, 2012], as illustrated by our reference simulation

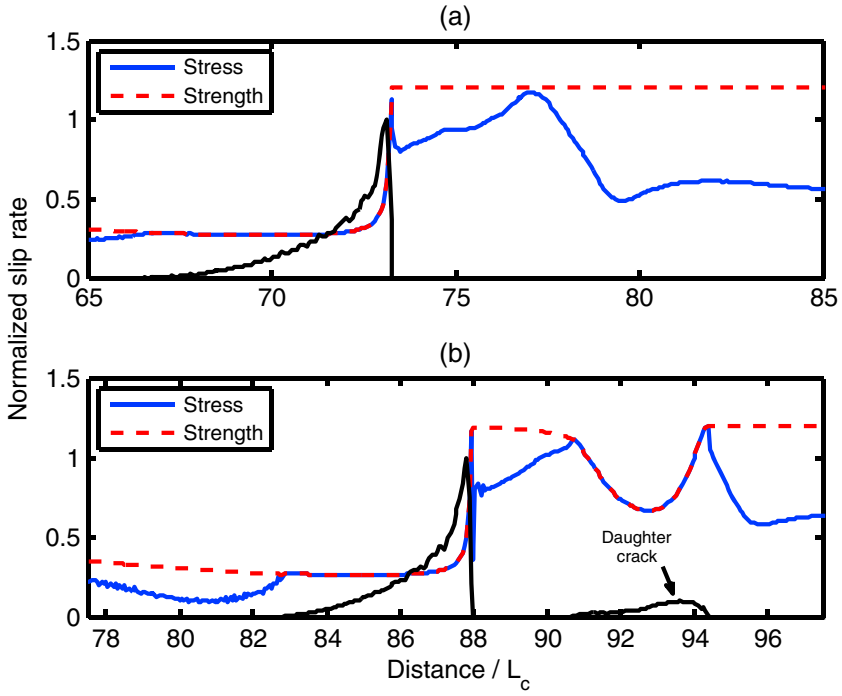

Figure 5. Slip rate, stress, and frictional strength (a) before and (b) after the supershear transition for ruptures in fault zones of 30% velocity reduction with a fault zone width of 16 L_c. Slip rate is normalized by the local peak slip rate.

(Figure 2). Fault zone waves hence promote supershear ruptures, as first noted by *Huang and Ampuero* [2011]. For the limit case when W^{FZ} increases to infinity, the problem converges to another homogeneous case with the elastic properties of the fault zone material, and hence, rupture speed approaches the Rayleigh wave speed of the fault zone and does not undergo oscillations anymore. Thus, there is an intermediate range of fault zone widths that promote supershear rupture. The disappearance of supershear ruptures as W^{FZ} increases beyond a certain level is related to the decay of the amplitude of fault zone waves with propagation distance due to geometric spreading (section 4). Moreover, we find that the supershear transition in fault zones operates through the same daughter crack mechanism as in homogeneous media [*Andrews*, 1976; *Dunham*, 2007]. Figures 5a and 5b show the slip rate, fault stress, and fault strength before and after the supershear transition in the case with $W^{FZ} = 16\ L_c$. A wave-mediated shear stress peak travels ahead of the initial rupture front. When it overcomes the fault strength, a daughter crack nucleates and eventually propagates spontaneously at a supershear speed close to v_p^{FZ} (Figure 5b).

3.4. Dependence of Rupture Speed, Rise Time, and Rupture Complexity on Velocity Contrast

As shown above, the amount of velocity reduction within the fault zone influences the fundamental properties of earthquake ruptures, e.g., it controls whether a rupture behaves as a steady state pulse or has oscillating rupture speed. To illustrate the fundamental differences between ruptures in fault zones and in homogeneous media, we summarize in Figure 6 the dependence of rupture speed and rise time on velocity reduction Δv when $W^{FZ} = 4\ L_c$. We consider rupture speed and rise time beyond a distance of 5 L_{nuc} from the hypocenter, well beyond transients related to the artificial nucleation procedure. We consider the rise time of the first pulse, which accomplishes more than 80% of the final slip after the initial oscillation of rupture speed or the transition to steady state rupture.

We identify two distinct rupture behaviors. When Δv = 20%–40%, rupture speed and rise time are highly oscillatory throughout the whole rupture process (Figure 6). When Δv = 60%–80%, rupture evolves to a steady state with rupture speed approaching v_p^{FZ} and rise time equal to about a half of W^{FZ}/v_s^{FZ} (Figures 6 and 7c). In the intermediate range, Δv = 40%–60%, ruptures are complicated yet interesting. For Δv between 40% and 50%, ruptures display a transition from pronounced periodic oscillations to damped oscillations

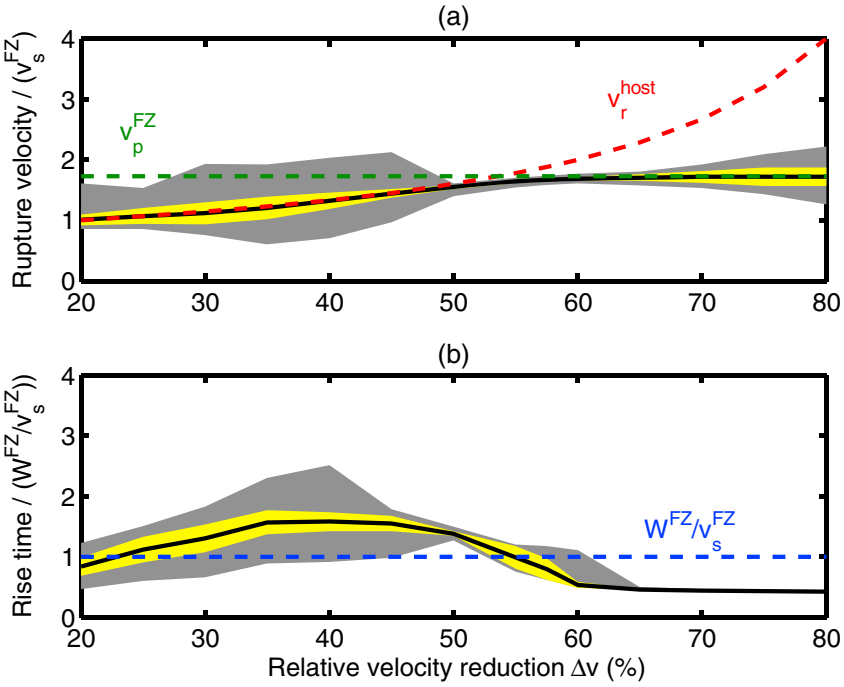

Figure 6. The total range (gray region), median (black solid line), and median absolute deviation (yellow region) of (a) rupture speed and (b) rise time in fault zones of different velocity contrasts when the fault zone width is 4 L_c. Green dashed line denotes *P* wave speed in the fault zone v_p^{FZ} and red dashed line denotes rupture speed in a homogeneous medium v_r^{host}, as shown in the reference simulation (Figure 2). Rupture speed is normalized by the *S* wave speed in the fault zone v_s^{FZ}, and rise time is normalized by the traveltime of fault normal reflected *S* waves W^{FZ}/v_s^{FZ} (blue dashed line).

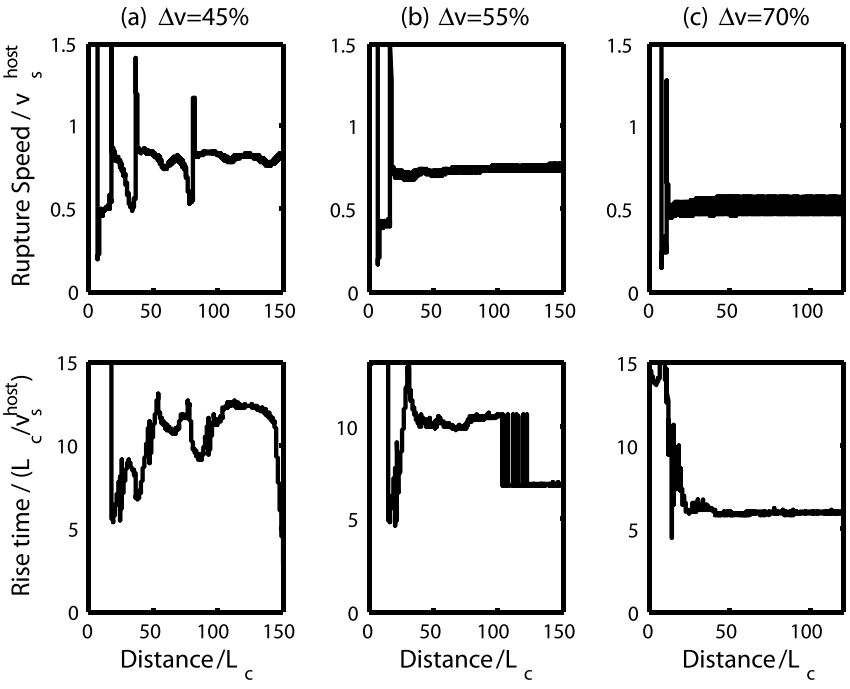

Figure 7. (top) Rupture speed and (bottom) rise time in fault zones of (a) 45%, (b) 55%, and (c) 70% velocity reductions with a fault zone width of 4 L_c.

(Figure 7a), which occurs earlier at larger Δv. When Δv = 50%–60%, rupture speed becomes steady very soon after rupture initiation but rise time does not. Instead, it drops (by less than a half) at a finite propagation distance (Figure 7b), which is shorter at larger Δv.

Because the maximum rupture speed appears to reach ~2.1 v_s^{FZ} (or ~1.2 v_s^{host}), it is tempting to say that ruptures can accelerate to a speed faster than v_s^{host} during the oscillations (Figure 4a and 4b). However, some of these supershear episodes may be too short-lived to be seismologically observable. Moreover, the estimates of rupture speed and rise time in dynamic rupture simulations are somewhat dependent on the measurement method and the degree of smoothing. Given that rupture speed and rise time vary during rupture propagation, we assess the overall rupture behavior by reporting their median and median absolute deviation in each simulation (black solid lines and yellow regions in Figures 6a and 6b). We find that, when $W^{FZ} = 4\ L_c$, ruptures are overall subshear with respect to the host rock, despite the oscillations of rupture speed: the median rupture speed stays at either v_p^{FZ} or v_r^{host}, whichever is lower (Figure 6a).

Because $v_r^{host} \approx 0.8\ v_s^{host}$ in our reference model, the median rupture speed is expected to stay at v_r^{host} when $\Delta v < \left(1 - v_r^{host}/v_p^{host}\right)$ = 53.8% and to approach v_p^{FZ} when $\Delta v > 53.8\%$. We can generalize this argument for different states of stress and friction parameters as long as v_r^{host} is known. For example, if the conditions are such that a rupture in a homogeneous medium propagates at the Rayleigh wave speed of the host rock (~0.92 v_s^{host}), the rupture speed in a fault zone is controlled by v_p^{FZ} if $\Delta v > \left(1 - 0.92 v_s^{host}/v_p^{host}\right) = 46.9\%$. Rupture speed transition occurs at a higher Δv if the rupture in a homogeneous medium is slower. Given the most common range of Δv in natural fault zones (~30–50%), rupture is more likely to be controlled by v_r^{host} under subshear conditions.

4. Fault Zone Waves and Their Influence on Rise Time and Rupture Speed

Our previous results indicate that fault zone waves are the key to understand the influence of fault zones on earthquake ruptures. To analyze the wavefield developed inside fault zones, we impose a kinematic "point" source and record the resulting perturbations of shear stress on the fault. The point source is approximated by a Gaussian slip rate function. The time duration of the slip rate function is chosen short enough to resolve characteristic phases of fault zone waves. The source amplitude is also spatially distributed as a Gaussian function with a width much smaller than the fault length yet large enough to ensure numerical resolution. For convenience of defining waves, we denote the material of the host rock as #1 and that of the fault zone as #2 (Figure 1). Thus, reflected waves that only involve *S* waves in the fault zone are referred to as S_2S_2, and *S* head waves that propagate at v_s^{host} along the boundary of the fault zone are referred to as $S_2S_1S_2$.

We identify different phases of reflected waves at early times (Figure 8a). The direct P_2 wave is followed by P_2P_2 reflected waves and then S_2P_2 and P_2S_2 reflected waves. Their speeds all approach v_p^{FZ} far from the source. The direct S_2 wave, which induces larger amplitude of stress perturbation than the *P* phases, is followed by S_2S_2 reflected waves. Beyond the distance at which reflected waves reach critical angles, head waves are generated and interfere with reflected waves (Figure 8b). The interference causes the polarity of head waves to alternate. Generally speaking, *S* head waves have longer period than *P* head waves.

We focus on the steady state ruptures (Δv = 60–80%) to understand the role of fault zone waves in generating slip pulses. As the steady state ruptures propagate at a speed of v_p^{FZ}, the waves that generate healing of the first pulse should approach the same speed in order to keep the rise time constant. Possible waves are P_2P_2, S_2P_2, and P_2S_2 reflected waves and $S_2P_2S_2$ head waves. We measure the differences of traveltime between the direct P_2 wave and the above waves. We find that only S_2P_2 and P_2S_2 reflected waves lead to a traveltime difference equal to the observed rise time of the first pulse (Figure 9). We also confirm that the stress perturbations caused by S_2P_2 and P_2S_2 reflected waves are unfavorable for slip, which is necessary to induce healing (Figure 8a). Thus, the S_2P_2 and P_2S_2 reflected waves generate the first pulses and control the rise time of steady state pulse-like ruptures. Moreover, as S_2P_2 and P_2S_2 reflected waves are nearly critical when their apparent speeds approach v_p^{FZ}, we have $v_p^{FZ} \approx v_s^{FZ}/\sin(\theta)$, where θ is the incidence or reflection angle of *S* waves. The rise time can be approximated

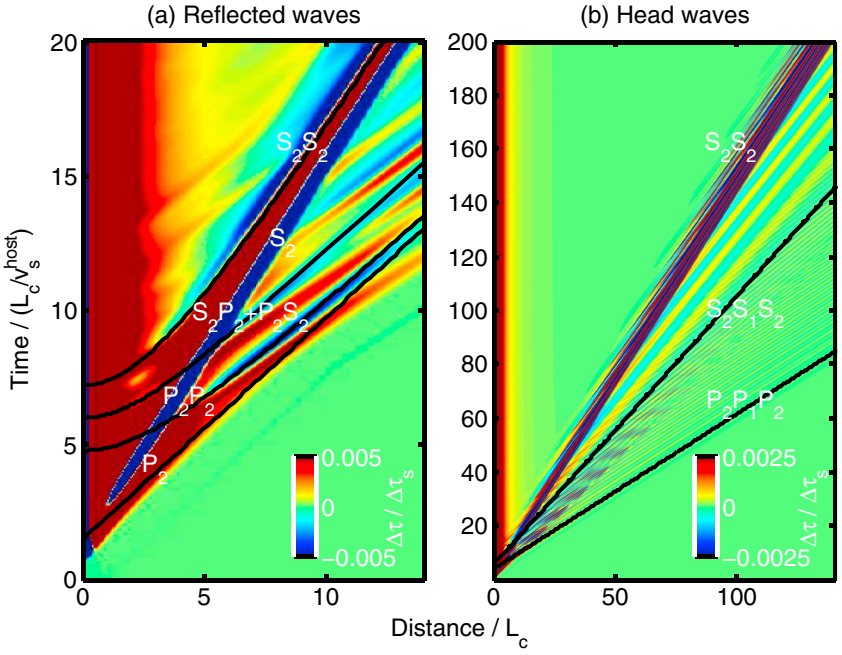

Figure 8. Spatiotemporal distribution of shear stress transient on the fault induced by a prescribed localized slip source at the hypocenter in a fault zone of 30% velocity reduction with a fault zone width of 4 L_c. Different phases of (a) reflected waves and (b) head waves are indicated.

by the traveltime difference between the rupture front and reflected wave. For nearly critical S_2P_2 and P_2S_2 reflected waves

$$\tau_{\text{ris}} \approx \left(\frac{W^{\text{FZ}}}{2\cos\theta v_s^{\text{FZ}}} + \frac{2L - W^{\text{FZ}}\tan\theta}{2v_p^{\text{FZ}}} \right) - \frac{L}{v_r} \tag{11}$$

where L and v_r are rupture length and rupture speed, respectively. Given $v_r = v_p^{\text{FZ}}$ and $\sin\theta = \frac{v_s^{\text{FZ}}}{v_p^{\text{FZ}}}$,

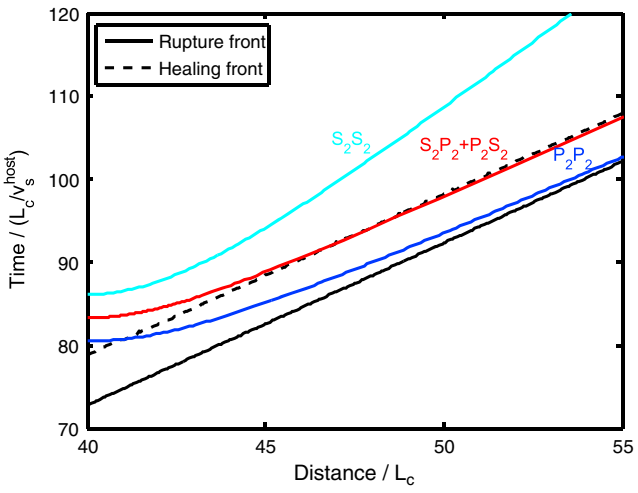

Figure 9. Rupture front and healing front of the rupture in a fault zone of 70% velocity reduction with a fault zone width of 4 L_c. The time difference between rupture front and healing front is the rise time. Traveltime curves of reflected waves are shown in color.

$$\tau_{\text{ris}} = \frac{W^{\text{FZ}}}{2v_s^{\text{FZ}}} \sqrt{1 - \left(\frac{v_s^{\text{FZ}}}{v_p^{\text{FZ}}} \right)^2} \approx 0.41 \frac{W^{\text{FZ}}}{v_s^{\text{FZ}}} \tag{12}$$

This equation is in good agreement with our numerical results, in which the rise time of steady state ruptures is about a half of $W^{\text{FZ}}/v_s^{\text{FZ}}$ (Figure 6b). Additional insight on dynamic stresses induced by steady pulses may be gained from the analytical work by *Weertman* [2014].

Fault zone waves can also accelerate and decelerate ruptures when Δv = 20–40% (Figures 4a, 4b, and 6a). We find that oscillations of the rupture front are caused by head waves. Accelerations of rupture front happen when head waves that carry a favorable stress perturbation arrive, and decelerations occur when

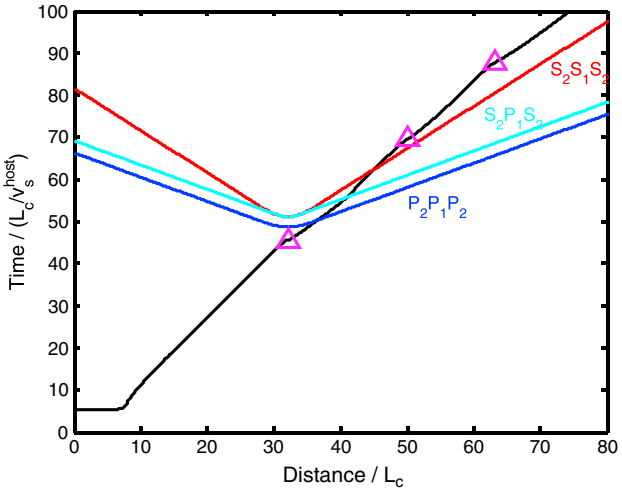

Figure 10. Rupture front of the rupture (black solid line) in a fault zone of 30% velocity reduction and fault zone width of 4 L_c. Magenta triangles denote the rupture acceleration episodes. Traveltime curves of the first arrivals of head waves radiated from the first acceleration episode are shown in color.

head waves with opposite polarity arrive. To understand whether *P* or *S* head waves control the period of oscillations, we mark each rupture acceleration episode on a space-time plot of the rupture front (W^{FZ} = 4 L_c, Figures 10 and 11) and then draw the traveltime curves of different head waves emanating from the first acceleration event. We find that the traveltime curve of the first arrival of $S_2S_1S_2$ head waves intersects the rupture front at a location closer to the second acceleration event than any of the other head waves (Figure 10). Such correlation is also valid for the other acceleration events (Figure 11). Note that we only plot the first arrivals of head waves based on ray theory, but the head waves with the largest amplitude actually arrive later (Figure 8b) with a delay influenced by the width of the fault zone and the characteristic frequency of the head waves. This explains why the period of oscillations increases nonlinearly with the increase of fault zone width (Figure 5c). Even considering such complexity, it is clear that the $S_2S_1S_2$ head waves induce acceleration of the rupture front and control the period of oscillations. However, both *P* and *S* head waves contribute to the onset of rupture acceleration, as we will discuss later in section 5.1.

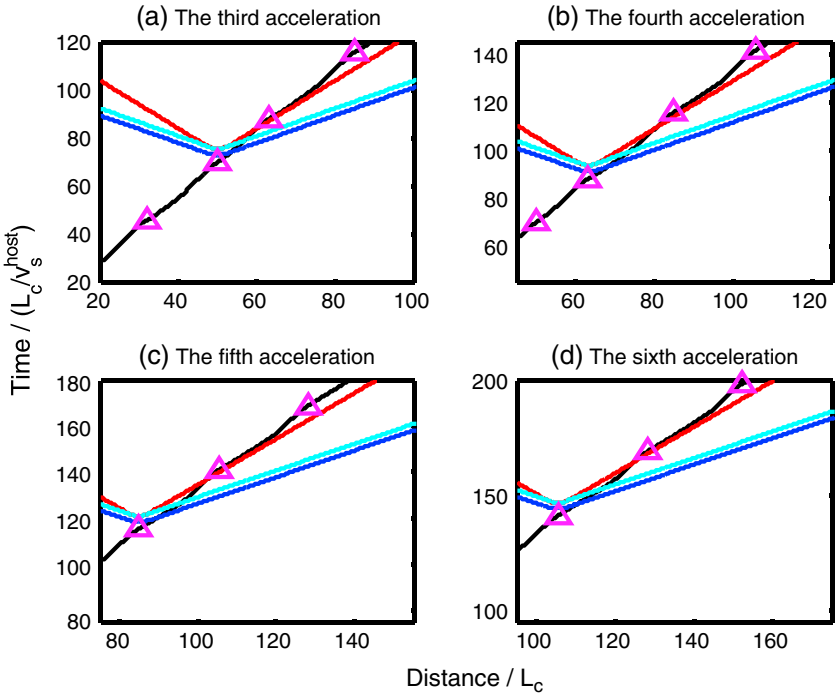

Figure 11. The correlation between the first arrivals of $S_1S_2S_1$ head waves (red solid lines) and the third to sixth acceleration events for the rupture in a fault zone of 30% velocity reduction and fault zone width of 4 L_c. Traveltime curves of the first arrivals of $P_2P_1P_2$ and $S_2P_1S_2$ head waves are shown in blue and turquoise, respectively. Magenta triangles denote the rupture acceleration episodes.

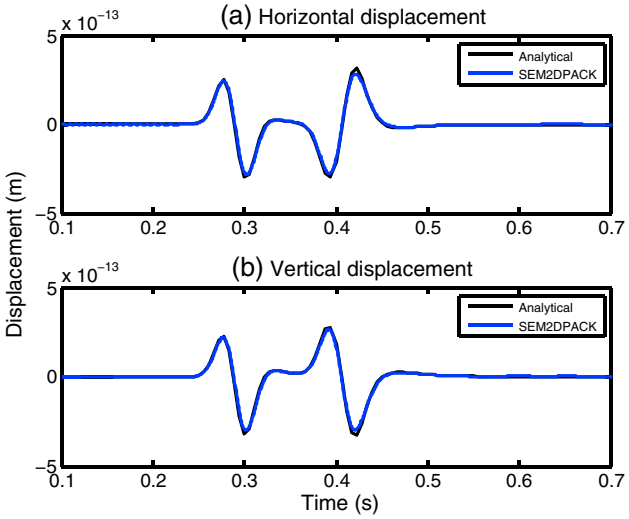

Figure 12. (a) Horizontal and (b) vertical displacements in a benchmark attenuation problem calculated by analytical solutions (black line) and SEM2DPACK with three inelastic functions (blue line). Given a vertical force source, the displacements are measured for a receiver located at $x = z = 500$ m, when x and z are distances along and across the fault from the hypocenter, respectively.

The effects of the fault zone velocity reduction on the wavefield also lead to complicated rupture behaviors in the transition regime (Δv = 40–60%). In addition to the $S_2S_1S_2$ head waves, $P_2S_1P_2$ head waves are also generated at the fault zone interface and propagate at v_s^{host} when $v_p^{\text{FZ}} < v_s^{\text{host}}$ ($\Delta v > 42.3\%$). The interference of $P_2S_1P_2$ and $S_2S_1S_2$ head waves diminishes the amplitude of $S_2S_1S_2$ head waves and hence their capacity to induce oscillations of rupture speed. Thus, the oscillations become damped and finally disappear if the velocity reduction is larger than 50%. When $\Delta v > 53.8\%$, rupture speed is solely controlled by the P wave speed inside the fault zone, and waves that propagate at v_p^{FZ} and carry unfavorable stresses start to compete for rupture healing. When $\Delta v > 60\%$, the S_2P_2 and P_2S_2 reflected waves prevail and maintain the rise time equal to about a half of $W^{\text{FZ}}/v_s^{\text{FZ}}$.

5. Ruptures in Inelastic Fault Zones

5.1. Ruptures in Fault Zones With Attenuation

Natural fault zones have a more complex mechanical behavior than a purely elastic medium. Seismic waves propagating through damaged materials are attenuated due to scattering and absorption of energy. Studies of seismic guided waves suggest that Q inside fault zones is in the range of 10 to 60 for S waves (Table 1) although there is a trade-off between the estimations of fault zone width, velocity, and Q [*Ben-Zion*, 1998]. However, the potential effects of attenuation on earthquake rupture dynamics remain largely unexplored. Reflected waves in fault zones have a characteristic frequency of several hertz and may be severely attenuated if Q is low. Thus, it is crucial to assess the effects of attenuation on ruptures in fault zones.

Following *Moczo et al.* [2004], we incorporate attenuation by adding viscoelastic terms in the stress-strain relations:

$$\sigma(t) = M_u \cdot \varepsilon(t) - \sum_{l=1}^{n} M_u Y_l \zeta_l(t) \tag{13}$$

$$\dot{\zeta}_l(t) + \omega_l \zeta_l(t) = \omega_l \varepsilon(t) \tag{14}$$

where M_u, Y_l, $\zeta_l(t)$, and ω_l are the unrelaxed modulus, anelastic coefficient, anelastic function, and relaxation frequency of the l^{th} viscoelastic mechanism, respectively. Seismic observations suggest that the quality factor Q is nearly constant over a certain frequency range [*Aki and Richards*, 2002]. To realize an approximately flat Q in a numerical method, an adequate number of anelastic functions $\zeta_l(t)$ and relaxation frequencies ω_l are needed to cover the frequency range under interest. We find that three anelastic functions are sufficient to obtain a practically constant Q, with relative error less than 5%, over a broad frequency band with maximum

Table 3. Model Parameters in Models With Attenuation

ρ (kg/m^3)	v_p^{host} (km/s)	v_s^{host} (km/s)	σ_0 (MPa)	τ_0 (MPa)	μ_s	D_c (m)	v_c (m/s)	a	b
2670	6.0	3.464	100	28.5	0.6	0.5	0.8	0.005	0.505

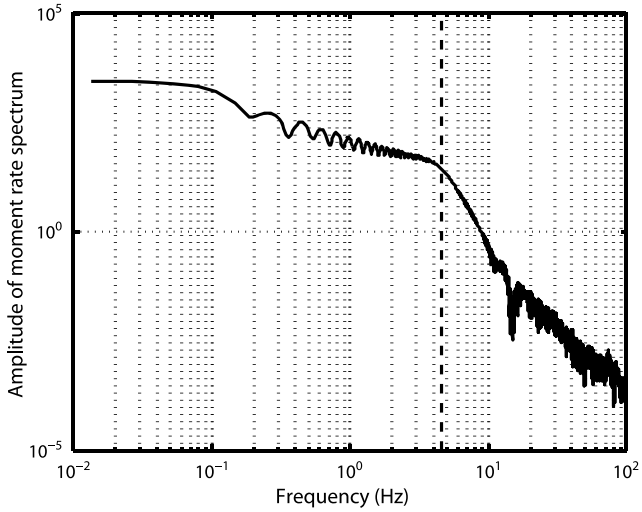

Figure 13. Moment rate spectrum of rupture in a 200 m wide fault zone with 50% velocity reduction when $Q = \infty$. The black dash-dotted line denotes the frequency equal to 4.6 Hz.

to minimum frequency ratio of 100. Anelastic coefficients can then be solved from the following equation given a certain frequency band ω:

$$Q^{-1}(\omega) = \sum_{l=1}^{n} \frac{\omega_l \omega + \omega_l^2 Q^{-1}(\omega)}{\omega_l^2 + \omega^2} Y_l \quad (15)$$

The unrelaxed modulus is calculated from the anelastic coefficients and phase velocity [*Moczo et al*., 2004, equations (166) and (167)]. We benchmarked our implementation by reproducing an example presented by *Komatitsch and Tromp* [1999] and compared our results to the analytical solutions by *Carcione et al*. [1988]. The benchmarked model has a constant Q_p = 30 and Q_s = 20 over a frequency band of 1.8–180 Hz centered at 18 Hz, which is also the dominant source frequency. Overall, our numerical results agree well with the analytical solutions (Figure 12).

We first illustrate the effects of attenuation on rise time by considering a 200 m wide fault zone with 50% velocity reduction. The material, stress, and friction parameters are shown in Table 3. We present simulations with three different values of Q applied to both P and S waves: $Q = \infty$ (no attenuation), 40, and 10. When $Q = \infty$, the rupture has significant power up to ~4.6 Hz, above which the moment rate spectrum is less than 1% of its maximum (Figure 13). This corner frequency is close to a half of the characteristic frequency of S waves in fault zones (v_s^{FZ}/W^{FZ} = 8.66 Hz). For simulations with Q = 40 and 10, we prescribe an almost constant Q from 0.1 to 10 Hz, which covers the dominant frequency range of the rupture. We find that rupture speeds hardly change with the decrease of Q: the reduction of rupture speeds is less than 2% from $Q = \infty$ to Q = 10. Attenuation has a stronger effect on the shape of slip pulses (Figure 14). When $Q = \infty$ (equivalent to a purely elastic medium), slip alternately stops and resumes at the arrival of each group of reflected waves. When Q = 10, the multiple slip pulse episodes behind the first pulse merge into a single pulse modulated by damped oscillations. Thus, attenuation reduces the efficiency of reflected waves to unload the fault. However, peak slip rate of slip pulses in the three cases is still significantly larger than that in a homogeneous medium, and the period of the slip rate oscillations is largely unaffected by attenuation.

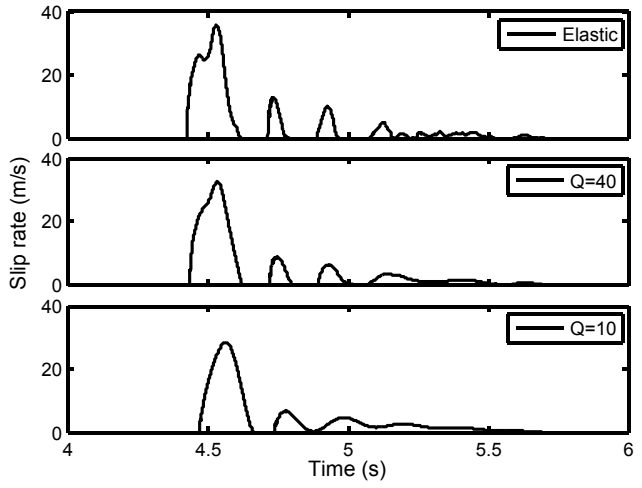

Figure 14. Slip rate functions at a distance of 14 km from the hypocenter for ruptures in 200 m wide fault zones with 50% velocity reduction and different Q.

Attenuation also influences the amplitude of head waves, which in turn can diminish their effect on oscillations of rupture speed. We illustrate this effect by considering a 1.6 km wide fault zone with 40% velocity reduction. As Q decreases, the first rupture acceleration episode beyond nucleation (marked by blue arrows in Figure 15) is postponed, but a reduced Q does not lead to an obvious increase of the oscillation period (Figures 15a, 15b, and 15c). The average oscillation period for different Q remain within 10% of each other. The amplitude of oscillations is severely reduced when

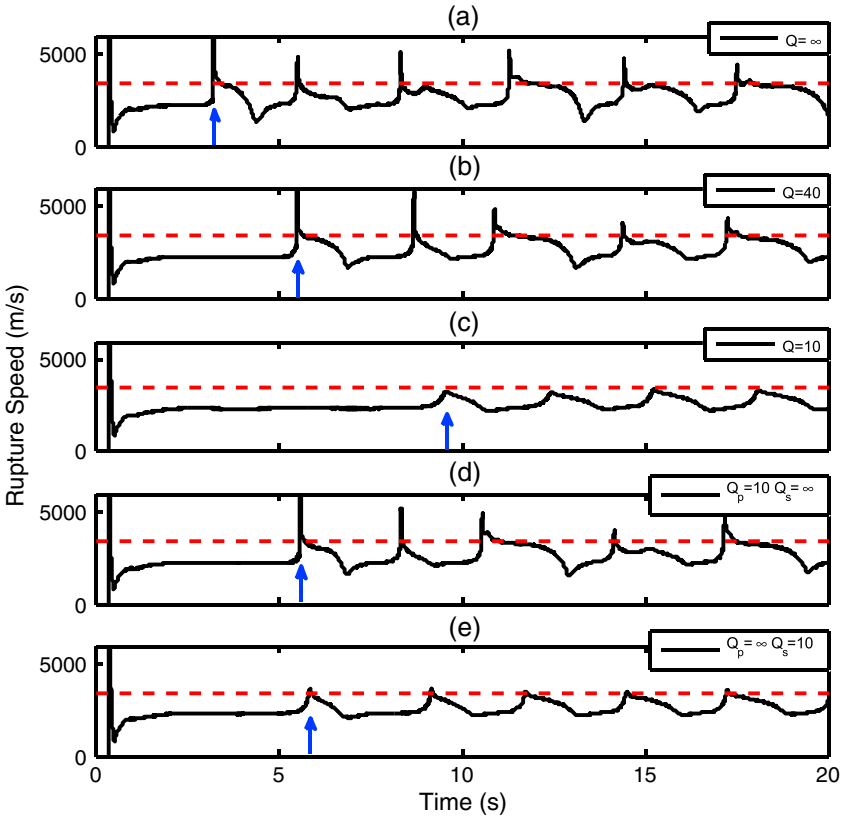

Figure 15. (a–e) Rupture speed as a function of time for ruptures in fault zones of different Q. Similar to the previous elastic cases, rupture speeds are measured based on the position and timing of the tail of the process zone. Red dashed lines denote v_s^{host}, and blue arrows mark the first rupture acceleration beyond nucleation.

Q = 10. To find out how P and S head waves affect the first rupture acceleration episode, we examine cases when either Q_p or Q_s is reduced. By comparing Figures 15d and 15e to Figure 15a, we find that the first rupture episode beyond nucleation is postponed when either Q_p or Q_s is reduced, which suggests that both P and S head waves as well as their conversions contribute to the onset of rupture acceleration.

Overall, the strong effect of attenuation on the shape of the slip rate functions and its weak effect on rupture speed and rupture oscillation period is consistent with the fact that attenuation strongly affects wave amplitude but not wave speed.

5.2. Ruptures in Fault Zones With Off-Fault Plasticity

Damaged materials inside fault zones probably undergo plastic deformation during earthquakes. Previous simulations show that plastic deformation tends to occur on the extensional side of the fault in a homogeneous medium, except when the maximum principal compressive stress is oriented at an angle smaller than ~20° to the fault [*Andrews*, 2005; *Templeton and Rice*, 2008; *Dunham et al*., 2011]. *Duan* [2008] studied the effect of fault zones with off-fault plasticity on dynamic ruptures and found plastic strain distributed on the extensional side. However, he assumed the same uniform background stress within and outside fault zones, which violates the boundary conditions at the interface between the fault zone and the host rock [*Casey*, 1980]. Reductions of elastic moduli in damaged fault zones in general induce rotation of the background stresses [*Faulkner*, 2006], which may generate different distributions of off-fault plastic deformation inside and outside fault zones. The generation of plastic deformation inside fault zones can affect rupture propagation and the mechanism of slip pulses. Also, plastic deformation can leave useful signatures on geological records and provide constraints on tectonic stresses [*Di Toro et al*., 2005; *Ben-Zion et al*., 2012]. Thus, it is worthwhile to reexamine dynamic rupture simulations inside fault zones with off-fault plasticity under mechanically consistent background stress.

Table 4. Model Parameters in Models With Off-Fault Plasticity

ρ (kg/m^3)	v_p^{host} (km/s)	v_s^{host} (km/s)	σ_0 (MPa)	τ_0(MPa)	μ_s	D_c(m)	v_c (m/s)	a	b
2670	6.0	3.464	100	32.22	0.6	0.25	0.8	0.005	0.505

We use the 2-D Mohr-Coulomb failure criterion for the onset of off-fault yielding. For a given cohesion c and internal coefficient of friction tan ϕ, failure happens when the maximum shear stress $\tau_{\max} = \sqrt{\sigma_{xz}^2 + [(\sigma_{xx} - \sigma_{zz})/2]^2}$ reaches the Coulomb threshold:

$$\tau_{\max} \geq c\cos\phi - \frac{1}{2}(\sigma_{xx} + \sigma_{zz})\sin\phi \tag{16}$$

After the onset of off-fault yielding, plastic strain cumulates. Viscoplastic regularization is introduced to stabilize numerical solutions [*Andrews*, 2005; *Xu et al*., 2012; *Gabriel et al*., 2013]. The angle between the maximum principal compressive stress and the fault plane Ψ is determined by:

$$\Psi = \frac{1}{2}\tan^{-1}\left[\frac{2\sigma_{xz}}{\sigma_{zz} - \sigma_{xx}}\right] \tag{17}$$

When Ψ is fairly small (<~20°), off-fault plastic strain is concentrated in the compressive side of the fault. Otherwise, it mostly happens on the extensional side. This asymmetry of plastic deformation is valid when Ψ is uniform throughout the medium. However, stress is certainly not uniform in a medium with fault zones. The interface between the fault zone and host rock needs to satisfy the following conditions [*Casey*, 1980; *Faulkner et al*., 2006]:

$$\sigma_{zz}^{host} = \sigma_{zz}^{FZ} \tag{18}$$

$$\sigma_{xz}^{host} = \sigma_{xz}^{FZ} \tag{19}$$

$$\dot{\varepsilon}_{xx}^{host} = \dot{\varepsilon}_{xx}^{FZ} \tag{20}$$

where x and z are fault-parallel and fault-perpendicular directions, respectively (Figure 1). Thus, the boundary conditions require a rotation of regional stresses in the medium. This stress rotation causes a change of Ψ from the host rock to the fault zone, which can break the pure asymmetry of plastic deformations.

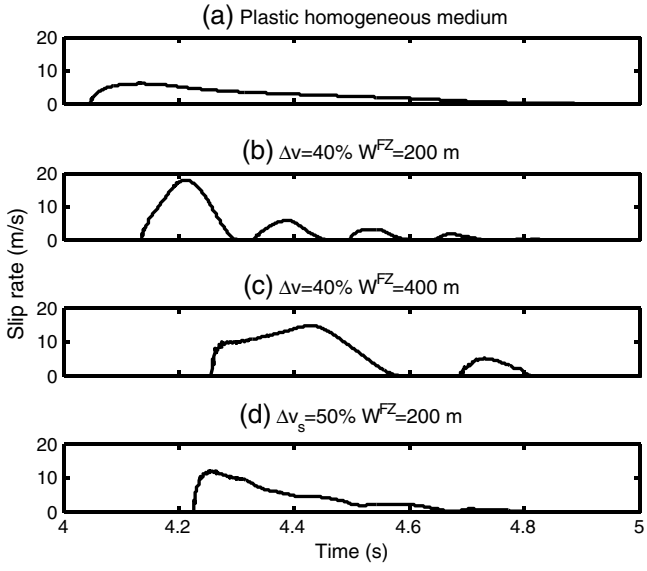

Figure 16. Slip rate functions at a distance of 9 km from the hypocenter for ruptures in (a) a homogeneous medium with off-fault plasticity and plastic fault zones of 40% velocity reduction with fault zone widths of (b) 200 m and (c) 400 m and (d) when only *S* wave velocity is reduced by 50% in the fault zone.

For simulations in this section, we employ a time-weakening nucleation procedure instead of an overstressed nucleation patch to avoid a discontinuity of Ψ along the fault. The size of the nucleation patch is prescribed to expand until half of the nucleation time and then shrink to zero [*Andrews and Ben-Zion*, 1997]. This nucleation procedure allows pulse-like ruptures to happen in a broad range of initial parameters [*Gabriel et al*., 2012]. Model parameters used in this section are shown in Table 4.

We first show a reference rupture simulation in a homogeneous medium with off-fault plasticity when Ψ = 14.27°. Rupture in a homogeneous medium propagates as a self-sustaining pulse beyond ~3 km (Figure 16a), half of the

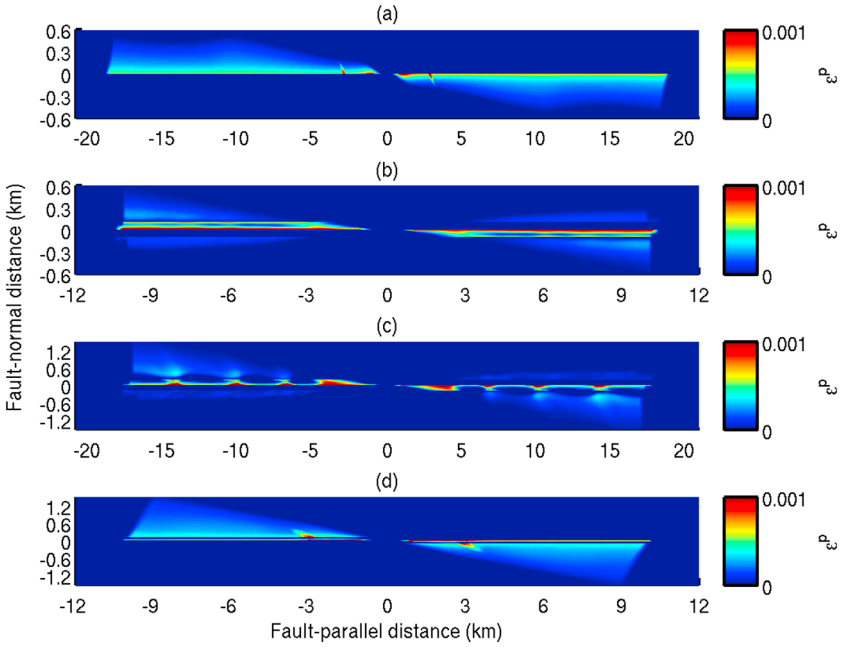

Figure 17. Plastic strain distributions in (a) a homogeneous medium and fault zones of 40% velocity reduction with fault zone widths of (b) 200 m and (c) 400 m and (d) when only *S* wave velocity is reduced by 50% in the fault zone.

prescribed nucleation size. A curvy-shaped yielding zone grows solely on the compressional side and saturates to a finite width (Figure 17a). This is similar to previous findings about off-fault plastic deformation of a pulse-like rupture in a homogeneous medium [*Xu et al.*, 2012].

We then consider a 200 m wide fault zone with 40% velocity reduction. The prestress angle Ψ rotates from 14.27° in the host rock to 45° within the fault zone. The rupture propagates as a sequence of multiple slip pulses (Figure 16b). Because $\Psi = 45°$ near the fault, the plastic yielding zone is located on the extensional side inside the fault zone (Figure 17b). This yielding zone also induces plastic deformation on the extensional side in the host rock, which forms a triangular-shaped yielding zone rather than a curvy-shaped one. Another yielding zone grows on the compressional side in the host rock, as expected for $\Psi = 14.27°$ from results in homogeneous media.

We further investigate a 400 m wide fault zone with 40% velocity reduction. Rise time of the first slip pulse (Figure 16c) is twice of that in a 200 m wide fault zone (Figure 16b), suggesting again the proportionality between rise time and W^{FZ}, as found for ruptures in elastic fault zones. Similar to the previous elastic cases, the oscillations of rupture speed become more pronounced as W^{FZ} increases. The intermittent accelerations of the rupture front induce highly concentrated off-fault plastic deformation, while decelerations only leave mild deformation (Figure 17c). Overall, the plastic yielding zone on the extensional side exhibits a spatially periodic pattern. This implies that ruptures in fault zones can leave a permanent and regular signature in the geologic record.

Seismic observations suggest that in natural fault zones the velocity reduction of *S* waves, Δv_s, is larger than that of *P* waves, Δv_p. For example, *Li et al.* [2007] suggest that $\Delta v_p \approx 42\%$ and $\Delta v_s \approx 58\%$ at a depth of 4.5 km. We consider an extreme case when only v_s^{FZ} is reduced by 50% and $\Psi = 50.8°$ in the host rock. The Poisson's ratio increases from 0.25 in the host rock to 0.45 inside the fault zone. As a result, the principal stress rotates to a direction more parallel to the fault plane ($\Psi = 45°$). Off-fault plastic deformation concentrates on the extensional side in both the fault zone and host rock (Figure 17d). The rupture propagates as a single pulse with damped oscillations instead of a train of multiple pulses (Figure 16d). This example shows the importance of Δv_p in the generation of slip pulses. Since the amplitude of P_2P_2 reflected waves is always favorable for slip, it also highlights the significant contributions of S_2P_2 and P_2S_2 reflected waves, as found for ruptures in elastic fault zones (section 4).

6. Discussion

Our numerical and theoretical results indicate the significant potential effects of fault zone waves on earthquake ruptures, even in the presence of attenuation and plasticity. Here we discuss these effects from the perspective of other plausible physical processes that may mitigate them or produce similar effects. We also highlight the significance of our findings from a broader perspective.

In our present study, we considered faults that bisect fault zones of uniform material properties. However, ruptures may also propagate along the boundary of fault zones [*Brietzke and Ben-Zion*, 2006] and, if the material contrast there is sharp, they can be viewed as bimaterial ruptures. More generally, ruptures can run anywhere off the middle plane of the fault zone and the resulting asymmetric configuration can be viewed as a generalized bimaterial rupture problem. Bimaterial ruptures can propagate as slip pulses, due to the dynamic change of normal stresses at the bimaterial interface [*Weertman*, 1980; *Ben-Zion and Huang*, 2002; *Ampuero and Ben-Zion*, 2008]. Thus, there is an inherent difference between our study and the studies of bimaterial ruptures. Moreover, given a large enough nucleation size and no matter how wide the fault zone is, we obtain sustained slip pulses. In contrast, sustained bimaterial pulses are found only when the nucleation size is smaller than the fault zone width [*Ben-Zion and Huang*, 2002]. Although our study and the bimaterial studies differ in some aspects, both find that fault zones can affect earthquake ruptures. For instance, the mild effect of fault zones on the modulation of slip rate was also identified in the bimaterial work of *Ben-Zion and Huang* [2002]. We note however that other fault zone effects studied here and in *Huang and Ampuero* [2011], including short rise times, oscillatory rupture speeds, and enhanced supershear transitions, are more drastic and hence more amenable for observation of real earthquakes. Overall, bimaterial ruptures and ruptures in symmetric fault zones studied in this paper are the two end-members of ruptures in asymmetric fault zones [*Dor et al*., 2006]. More work is certainly warranted to develop a complete understanding of the interaction between bimaterial effects and fault zone wave effects. This topic is also relevant for subduction megathrusts overlain by low-velocity sediment layers [*Rowe et al*., 2013].

Other mechanisms for the generation of slip pulses involve velocity-dependent friction [*Perrin et al*., 1995; *Beeler and Tullis*, 1996] and stress heterogeneities on the fault [*Beroza and Mikumo*, 1996]. Our current understanding of fault friction under seismic sliding velocity is mostly drawn from laboratory experiments as reviewed by *Di Toro et al*. [2011]. While laboratory results share some similarity with natural faulting, it is still a challenge to achieve the pressure, temperature, loading, and fluid conditions of the natural environment. Hence, large uncertainties remain about the frictional constitutive equations and parameters of natural faults at seismogenic depth. Stress conditions on the fault can be inferred from either fault roughness, which is limited to the scale of field observations [*Candela et al*., 2011], or focal mechanism studies, from which only smoothed distributions of stresses are available due to limited resolution [*Smith and Heaton*, 2011]. Thus, it is challenging to relate the properties of slip pulses to friction parameters or stress heterogeneities in nature. In comparison, the properties of fault zone structures have been thoroughly studied in many faults (Table 1). As inferred from Figure 6b, the range of the rise time of ruptures in fault zones is $\sim (0.5–2.5)\ W^{FZ}/v_s^{FZ}$. Because natural fault zones are usually 100 to 400 m wide (except for the Calico fault zone, which is ~1.5 km wide), the rise time of slip pulses caused by fault zone waves is in the order of 0.025–0.5 s given $v_s^{FZ} = 2$ km/s. While this range is consistent with higher bounds inferred from seismological observations [*Heaton*, 1990], to resolve the short slip pulses induced by natural fault zones it is necessary to develop observations at frequencies of several hertz that overcome the obstruction by attenuation and scattering in the Earth's crust and the uncertainties on crustal structure.

Two other dramatic effects of fault zones are oscillations of rupture speed and the enhancement of supershear rupture transitions. Previous numerical simulations of ruptures in fault zones under slip-weakening friction found supershear transitions enhanced within a certain range of fault zone widths [*Harris and Day*, 1997; *Huang and Ampuero*, 2011]. The current study, under strongly velocity weakening friction, confirms this finding and suggests a richer behavior of rupture speed. Because ruptures are more sensitive to stress perturbations under strongly velocity weakening friction, we see periodic oscillations of rupture speed in fault zones of 20%–40% velocity reductions. As the fault zone width increases, we find a switch to supershear rupture speed caused by head waves. We confirm through simulations that supershear ruptures indeed happen in fault zones of 30%–42% velocity reductions. Supershear transition is expected to occur later than the simulation time in fault zones of 20%–30% velocity reductions. Although we showed that the supershear transition in fault zones

operates via the same daughter crack mechanism as in homogeneous media, there are two main differences between supershear ruptures in a homogeneous medium and in fault zones. First, in fault zones supershear ruptures are possible even at stresses that are too low to allow supershear ruptures in a homogeneous medium. The increase of shear stresses caused by head waves is sufficient to trigger supershear rupture. Our work, combined with correlations between fault age and fault zone development [*Savage and Brodsky*, 2011], provides a mechanical rationale to interpret empirical correlations between the occurrence of supershear ruptures and other fault properties controlled by fault maturity, such as geometrical simplicity [*Bouchon et al*., 2010]. Specifically, our results suggest that supershear rupture is promoted by fault maturity because of the larger velocity reduction in the damaged fault zone. Second, as supershear ruptures happen in fault zones of 20–42% velocity reductions and approach v_p^{FZ}, they can propagate steadily at (1–1.39) v_s^{host}, which is an unstable range of supershear rupture speeds in a homogeneous medium [*Das*, 2010]. Such unexpected rupture speeds have been recently identified in real earthquakes within the Big Bear and Newport-Inglewood fault zones [*Tan and Helmberger*, 2010; *Luo et al*., 2010; *Huang et al*., 2013]. The implications of these theoretical and observational results on our macroscopic understanding of the earthquake energy balance remain to be developed.

Several additional complexities need to be considered for earthquakes in natural fault zones. One primary uncertainty in nature is the fault stress. To achieve healing, the stress change induced by reflected waves in the fault zone needs to overcome the dynamic stress drop, $\tau_0 - \tau_d$. Such insight can be gained through the relation between fault shear stress τ, initial stress τ_0, and slip rate D':

$$\tau(x,t) = \tau_0(x) + \phi(x,t) - \frac{G}{2v_s} D'(x,t) \tag{21}$$

The term ϕ represents the stress transfer induced by elastodynamic waves radiated by previous slip [*Zheng and Rice*, 1998]. This term includes the stress induced by reflected waves in the fault zone. The last term is radiation damping [*Rice*, 1993], where G is shear modulus and v_s is shear wave speed. Well behind the rupture front $\tau \approx \tau_d$, and, in the absence of reflected waves, the mild slip rate gradient renders ϕ small. At the arrival of the reflected waves, ϕ becomes dominated by their unloading stresses, and the frictional strength remains near τ_d because slip decelerates too quickly for the state variable to evolve significantly. Slip arrest ($D' = 0$) then requires $\tau_0 < \tau_d$, and hence, the stress perturbation induced by reflected waves must satisfy $-\phi > \tau_0 - \tau_d$. The peak stress carried by a wave radiated by the rupture front and reflected at the fault zone boundary scales with the strength drop in the process zone, $\tau_s - \tau_d$. It is further affected by factors controlled by fault zone properties, including reflection coefficient, geometrical spreading, and attenuation. At background shear stresses lower than in the simulations presented here (relative to the strength drop), the stress drops that reflected waves need to counteract to enable healing are also smaller compared to the peak stresses carried by reflected waves, and thus, the generation of slip pulses is more robust [*Huang and Ampuero*, 2011, Figure 6]. For instance, we expect pulses at lower stress to be less affected by attenuation. Thus, the fault zone wave mechanism for slip pulses should be robust for natural faults that have mature fault zones and operate at low fault stress, e.g., the San Andreas fault. We note however that the fault zone pulse mechanism is not sufficient to achieve low absolute shear stresses consistent with the low heat flow near the San Andreas fault; that still requires severe frictional weakening.

Our findings of multiple slip pulses and oscillatory rupture velocity are based on a fault zone model with well-defined boundaries manifested by abrupt wave velocity contrasts. In natural fault zones, a seismological diagnostic of such sharp boundaries is the presence of multiple reflections in high-frequency body waves from small earthquakes, as observed in the Landers, San Jacinto, and Calico fault zones [*Li et al*., 2007; *Yang and Zhu*, 2010; *Yang et al*., 2011]. Seismic wave velocity logs collected in the SAFOD (San Andreas Fault Observatory at Depth) borehole also indicate abrupt changes of both *P* and *S* waves in the San Andreas fault zone [*Ellsworth and Malin*, 2011]. However, not all fault zones have sharp interfaces. For instance, borehole data from the Nojima fault show a progressive reduction of seismic wave velocities within the fault zone [*Huang and Ampuero*, 2011; *Johri et al*., 2014]. In such fault zones, multiple reflections and head waves do not exist, and hence, multiple slip pulses and oscillatory rupture velocity are not expected. We conduct three simulations with fault zones that have an exponential distribution of both *P* and *S* wave speeds as a function of fault-perpendicular distance z: $v(z) = v^{host}\left(1 - \Delta v_{max} e^{-\frac{5z}{W_{FZ}}}\right)$, where v^{host} is the *P*

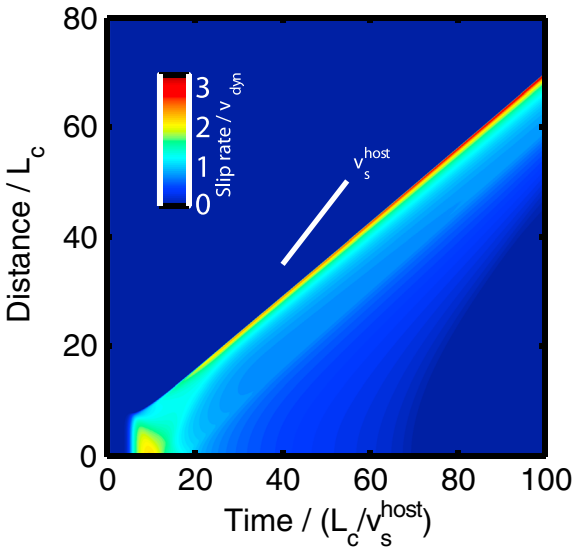

Figure 18. Spatiotemporal view of slip rate for a rupture in a fault zone with an exponential distribution of both *P* and *S* wave speeds as a function of fault-perpendicular distance. The simulation is for a fault zone with a maximum velocity reduction of 60% when $W^{FZ} = 2\ L_c$.

or *S* wave speed of the host rock and Δv_{max} is the maximum velocity reduction inside the fault zone (Figure 18). The three simulations have maximum velocity reductions of 40%, 60%, and 80% when $W^{FZ} = 2\ L_c$. We find ruptures in fault zones of larger velocity reductions feature lower rupture speeds and slip pulses with larger peak slip rate and longer rise time. Rupture speeds in all three simulations are steady and slower than the homogeneous rupture speed v_r^{host}. The peak slip rate of slip pulses in smooth fault zones is larger than that in a homogeneous medium due to reduced shear modulus. However, the periodicity of slip rate function and rupture speed does not exist in such fault zones with an exponential change of wave speeds.

More work remains to be done to assess the effect of heterogeneous fault zone structures, with nonplanar fault zone boundaries or nonuniform distributions of wave speed that may affect the constructive interference that controls the efficiency of the fault zone trapped waves. The width of a fault zone can vary significantly along strike, sometimes abruptly. The spatially periodic pattern of plastic deformation presented in section 5.2 also shows an example of coseismic inelastic process that can lead to along-strike variation of fault zone width. Geometrical irregularities can scatter fault zone waves away from the fault, but it may also produce focusing effects that contribute to rupture complexity. Scattering by small-scale 3-D heterogeneities of highly anisotropic statistical properties, with longer correlation length in the direction of rupture propagation, may also help guide high-frequency waves, as proposed for subducting slabs [*Furumura and Kennett*, 2008; *Chen et al*., 2013] and promote pulse-like rupture in subduction earthquakes. Whether the heterogeneity of fault zone structure is enhanced or reduced by further earthquakes is an important question that requires multiple earthquake cycle simulations with off-fault damage.

Three-dimensional effects can also mitigate the efficiency of fault zone waves. Unlike in 2-D, the amplitude of fault zone trapped waves in 3-D decays with propagation distance due to geometrical spreading. However, this decay is inversely proportional to the square root of distance, which is much weaker than the exponential decay due to attenuation. Hence, our 2-D simulations with attenuation contain a more severe mitigation ingredient than 3-D geometrical spreading, and yet they present significant effects of fault zone waves on rupture dynamics even with $Q = 10$. A variety of 3-D simulation results supporting these arguments will be reported elsewhere [*Pelties et al*., 2013].

Some of our results, for instance the conditions for supershear rupture but not the rise time and the period of rupture oscillations, depend on fault zone width through its ratio to the (static) process zone size, $W^{FZ}/L_c = W^{FZ}\sigma_0(\mu_s - \mu_d)/G^{host}D_c$. In other words, some aspects of a rupture are only affected by fault zone structures whose width is larger than the process zone size. The most uncertain parameter in this nondimensional number is D_c, the characteristic slip-weakening scale of the friction law. In elastic models, D_c may in reality represent a lumped parameter that encapsulates a variety of on-fault and off-fault dissipation processes and could be scale dependent (rupture length dependent), hence magnitude dependent. This view would suggest that small and large ruptures are not equally sensitive to the presence of preexisting fault zone structures [*Huang and Ampuero*, 2011] and that the sensitivity evolves during rupture growth. However, earthquake rupture can generate coseismically a damage zone whose width is sufficient to induce strong interactions with the rupture and affect the generation of slip pulses [*Xu et al*., 2009]. This suggests that the fault zone effects described here are not restricted to preexisting damage structures but their occurrence may be more universal.

7. Conclusions

Earthquakes are likely to happen in a heterogeneous medium. Fault zones are one form of heterogeneity that can have profound effects on earthquake ruptures. We find in this study that fault zone waves in low-velocity fault zones with sharp boundaries are responsible for the following effects. Reflected waves can heal the ruptures and cause slip pulses. Their dominant rise time is controlled by the fault zone properties rather than by the friction parameters. Head waves can accelerate the ruptures periodically and induce supershear transitions. The supershear ruptures can run at speeds that would be forbidden for stable ruptures in a homogeneous medium. As the amplitudes of fault zone waves depend on the velocity contrast of fault zones, we observe distinct rupture behaviors as a function of the degree of fault zone damage. In fault zones with 20–40% velocity contrast, ruptures propagate with pronounced speed oscillations or undergo a supershear transition. In fault zones with 60–80% velocity reduction, ruptures propagate as steady state pulses with constant rise time controlled by traveltime across the fault zone width. We find that the fault zone effects are mildly affected by attenuation: it affects the shape of slip pulses and delays the supershear transition, but it hardly alters rise time, slip rate, and rupture speed. The effects of fault zone waves also persist in the presence of off-fault plasticity. Unlike in homogeneous media, the formation of yielding zones in both sides of the fault is facilitated by the rotation of background stresses inside the fault zone. The oscillations of rupture speed lead to spatially periodic patterns of plastic deformation. Our studies provide new mechanisms for the generation of slip pulses and supershear transition. Our findings are considerably important to understand and guide seismic and field observations. In regions where fault zone structures are well characterized, the effects of fault zones should be taken into account for future studies.

Acknowledgments

This work was supported by the NSF (grants EAR-0944288 and EAR-1151926) and SCEC (funded by NSF EAR-0106924 and USGS 02HQAG0008 cooperative agreements). We thank the two reviewers and the Associate Editor for very helpful reviews. We also thank Eric Dunham for constructive comments and researchers who have done detailed observations of fault zone structures.

References

Aki, K., and P. G. Richards (2002), *Quantitative Seismology: Theory and Methods*, Univ. Science Books, Sausalito, Calif.

Ampuero, J.-P., and Y. Ben-Zion (2008), Cracks, pulses and macroscopic asymmetry of dynamic rupture on a bimaterial interface with velocity weakening friction, *Geophys. J. Int.*, *173*(2), 674–692, doi:10.1111/j.1365-246X.2008.03736.x.

Andrews, D. J. (1976), Rupture velocity of plane strain shear cracks, *J. Geophys. Res.*, *81*(32), 5679–5687, doi:10.1029/JB081i032p05679.

Andrews, D. J. (2005), Rupture dynamics with energy loss outside the slip zone, *J. Geophys. Res.*, *110*, B01307, doi:10.1029/2004JB003191.

Andrews, D. J., and Y. Ben-Zion (1997), Wrinkle-like slip pulse on a fault between different materials, *J. Geophys. Res.*, *102*(B1), 553–571, doi:10.1029/96JB02856.

Archuleta, R. J. (1984), A faulting model for the 1979 Imperial Valley earthquake, *J. Geophys. Res.*, *89*(B6), 4559–4585, doi:10.1029/JB089iB06p04559.

Beeler, N. M., and T. E. Tullis (1996), Self-healing slip pulses in dynamic rupture models due to velocity-dependent strength, *Bull. Seismol. Soc. Am.*, *86*(4), 1130–1148.

Beeler, N. M., T. E. Tullis, and D. L. Goldsby (2008), Constitutive relationships and physical basis of fault strength due to flash heating, *J. Geophys. Res.*, *102*, B01401, doi:10.1029/2007JB004988.

Ben-Zion, Y. (1998), Properties of seismic fault zone waves and their utility for imaging low-velocity structures, *J. Geophys. Res.*, *103*(B6), 12,567–12,585, doi:10.1029/98JB00768.

Ben-Zion, Y., and J.-P. Ampuero (2009), Seismic radiation from regions sustaining material damage, *Geophys. J. Int.*, *178*(3), 1351–1356, doi:10.1111/j.1365-246X.2009.04285.x.

Ben-Zion, Y., and Y. Huang (2002), Dynamic rupture on an interface between a compliant fault zone layer and a stiffer surrounding solid, *J. Geophys. Res.*, *107*(B2), 2042, doi:10.1029/2001JB000254.

Ben-Zion, Y., and C. G. Sammis (2003), Characterization of fault zones, *Pure Appl. Geophys.*, *160*(3–4), 677–715.

Ben-Zion, Y., Z. Peng, D. Okaya, L. Seeber, J. G. Armbruster, N. Ozer, A. J. Michael, S. Baris, and M. Aktar (2003), A shallow fault-zone structure illuminated by trapped waves in the Karadere-Duzce branch of the North Anatolian Fault, wester Turkey, *Geophys. J. Int.*, *152*(3), 699–717, doi:10.1111/j.1365-246X.2003.01870.x.

Ben-Zion, Y., T. Rockwell, Z. Shi, and S. Xu (2012), Reversed-polarity secondary deformation structures near fault stepovers, *J. Appl. Mech.*, *79*, 031025, doi:10.1115/1.4006154.

Beroza, G. C., and T. Mikumo (1996), Short slip duration in dynamic rupture in the presence of heterogeneous fault properties, *J. Geophys. Res.*, *101*(B10), 22,449–22,460, doi:10.1029/96JB02291.

Bouchon, M., and M. Vallee (2003), Observation of long supershear rupture during the magnitude 8.1 Kunlunshan earthquake, *Science*, *301*, 824–826, doi:10.1126/science.1086832.

Bouchon, M., M.-P. Bouin, H. Karabulut, M. N. Toksoz, M. Dietrich, and A. J. Rosakis (2001), How fast is rupture during an earthquake? New insights from the 1999 Turkey earthquakes, *Geophys. Res. Lett.*, *28*(14), 2723–2726, doi:10.1029/2001GL013112.

Bouchon, M., M. N. Toksoz, H. Karabulut, M.-P. Bouin, M. Dietrich, M. Aktar, and M. Edie (2002), Space and time evolution of rupture and faulting during the 1999 Izmit (Turkey) earthquake, *Bull. Seismol. Soc. Am.*, *92*(1), 256–266, doi:10.1785/0120000845.

Bouchon, M., H. Karabulut, M.-P. Bouin, J. Schmittbuhl, M. Vallee, R. Archuleta, S. Das, F. Renard, and D. Marsan (2010), Faulting characteristics of supershear earthquakes, *Tectonophysics*, *493*(3–4), 244–253, doi:10.1016/j.tecto.2010.06.011.

Brietzke, G. B., and Y. Ben-Zion (2006), Examining tendencies of in-plane rupture to migrate to material interfaces, *Geophys. J. Int.*, *167*(2), 807–819, doi:10.1111/j.1365-246X.2006.03137.x.

Candela, T., F. Renard, M. Bouchon, J. Schmittbuhl, and E. E. Brodsky (2011), Stress drop during earthquakes: Effects of fault roughness scaling, *Bull. Seismol. Soc. Am.*, *101*(5), 2369–2387, doi:10.1785/0120100298.

Carcione, J. M., D. Kosloff, and R. Kosloff (1988), Wave propagation simulation in a linear viscoelastic medium, *Geophys. J.*, *95*, 597–611.

Casey, M. (1980), Mechanics of shear zones in isotropic dilatant materials, *J. Struct. Geol.*, *2*(1/2), 143–147.

Chen, K. H., B. L. N. Kennett, and T. Furumura (2013), High-frequency waves guided by the subducted plates underneath Taiwan and their association with seismic intensity anomalies, *J. Geophys. Res. Solid Earth*, *118*, 665–680, doi:10.1002/jgrb.50071.
Chester, F. M., and J. S. Chester (1998), Ultracataclasite structure and friction processes of the Punchbowl fault, San Andreas system, California, *Tectonophysics*, *295*(1–2), 199–221.
Chester, F. M., and J. S. Chester (2000), Stress and deformation along wavy frictional faults, *J. Geophys. Res.*, *105*(B10), 23,421–23,430, doi:10.1029/2000JB900241.
Chester, F. M., and J. M. Logan (1986), Implications for mechanical properties of brittle faults from observations of the Punchbowl fault zone, California, *Pure Appl. Geophys.*, *124*(1–2), 79–106, doi:10.1007/BF00875720.
Childs, C., T. Manzocchi, J. J. Walsh, C. G. Bonson, A. Nicol, and M. P. J. Schopfer (2009), A geometric model of fault zone and fault rock thickness variations, *J. Struct. Geol.*, *31*(2), 117–127, doi:10.1016/j.jsg.2008.08.009.
Cochran, E. S., Y. G. Li, P. M. Shearer, S. Barbot, Y. Fialko, and J. E. Vidale (2009), Seismic and geodetic evidence for extensive, long-lived fault damage zones, *Geology*, *37*(4), 315–318, doi:10.1130/G25306A.1.
Cowie, P. A., and C. H. Scholz (1992), Physical explanation for the displacement length relationship of faults using a post-yield fracture mechanics model, *J. Struct. Geol.*, *14*(10), 1133–1148, doi:10.1016/0191-8141(92)90065-5.
Das, S. (2010), Earthquake supershear rupture speeds, *Tectonophysics*, *493*(3), 213–215, doi:10.1016/j.tecto.2010.07.009.
Das, S., and K. Aki (1977), A numerical study of two-dimensional spontaneous rupture propagation, *Geophys. J. R. Astron. Soc.*, *50*(3), 643–668, doi.10.1111/j.1365-246X.1977.tb01339.x.
Day, S. M. (1982), Three-dimensional finite difference simulation of fault dynamics: Rectangular faults with fixed rupture velocity, *Bull. Seismol. Soc. Am.*, *72*(3), 705–727.
Di Toro, G., S. Nielsen, and G. Pennacchioni (2005), Earthquake rupture dynamics frozen in exhumed ancient fault, *Nature*, *436*, 1009–1012, doi:10.1038/nature03910.
Di Toro, G., R. Han, T. Hirose, N. De Paola, S. Nielsen, K. Mizoguchi, F. Ferri, M. Cocco, and T. Shimamoto (2011), Fault lubrication during earthquakes, *Nature*, *471*, 494–499, doi:10.1038/nature09838.
Dor, O., T. K. Rockwell, and Y. Ben-Zion (2006), Geological observations of damage asymmetry in the structure of the San Jacinto, San Andreas and Punchbowl faults in southern California: A possible indicator for preferred rupture propagation direction, *Pure Appl. Geophys.*, *163*, 301–349, doi:10.1007/s00024-005-0023-9.
Duan, B. (2008), Effects of low-velocity fault zones on dynamic ruptures with nonelastic off-fault response, *Geophys. Res. Lett.*, *35*, L04307, doi:10.1029/2008GL033171.
Dunham, E. M. (2007), Conditions governing the occurrence of supershear ruptures under slip-weakening friction, *J. Geophys. Res.*, *112*, B07302, doi:10.1029/2006JB004717.
Dunham, E. M., and R. J. Archuleta (2004), Evidence for a supershear transient during the 2002 Denali Fault earthquake, *Bull. Seismol. Soc. Am.*, *94*(6B), S256–S268, doi:10.1785/0120040616.
Dunham, E. M., D. Belanger, L. Cong, and J. E. Kozdon (2011), Earthquake ruptures with strongly rate-weakening friction and off-fault plasticity. Part 1: Planar faults, *Bull. Seismol. Soc. Am.*, *101*(5), 2296–2307, doi:10.1785/0120100075.
Ellsworth, W. L., and P. E. Malin (2011), Deep rock damage in the San Andreas Fault revealed by P- and S-type fault-zone-guided waves, *Geol. Soc. London Spec. Publ.*, *2011*(359), 39–53, doi:10.1144/SP359.3.
Ellsworth, W. L., M. Celebi, J. R. Evans, E. G. Jensen, R. Kayen, M. C. Metz, D. J. Nyman, J. W. Roddick, P. Spudich, and C. D. Stephens (2004), Near-field ground motion of the 2002 Denali Fault, Alaska, earthquake recorded at Pump Station 10, *Earthquake Spectra*, *20*(3), 597–615, doi:10.1193/1.1778172.
Faulkner, D. R., T. M. Mitchell, D. Healy, and M. J. Heap (2006), Slip on 'weak' faults by the rotation of regional stress in the fracture damage zone, *Nature*, *444*, 922–925, doi:10.1038/nature05353.
Faulkner, D. R., T. M. Mitchell, E. Jensen, and J. Cembrano (2011), Scaling of fault damage zones with displacement and the implications for fault growth processes, *J. Geophys. Res.*, *116*, B05403, doi:10.1029/2010JB007788.
Furumura, T., and B. L. N. Kennett (2008), A scattering waveguide in the heterogeneous subducting plate, *Adv. Geophys.*, *50*(7), 195–217, doi:10.1016/S0065-2687(08)00007-1.
Gabriel, A.-A., J.-P. Ampuero, L. A. Dalguer, and P. M. Mai (2012), The transition of dynamic rupture styles in elastic media under velocity-weakening friction, *J. Geophys. Res.*, *117*, B09311, doi:10.1029/2012JB009468.
Gabriel, A.-A., J.-P. Ampuero, L. A. Dalguer, and P. M. Mai (2013), Source properties of dynamic rupture pulses with off-fault plasticity, *J. Geophys. Res. Solid Earth*, *118*, 4117–4126, doi:10.1002/jgrb.50213.
Goldsby, D. L., and T. E. Tullis (2011), Flash heating leads to low frictional strength of crustal rocks at earthquake slip rates, *Science*, *334*, 216–218, doi:10.1126/science.1207902.
Harris, R. A., and S. M. Day (1997), Effects of a low-velocity zone on a dynamic rupture, *Bull. Seismol. Soc. Am.*, *87*(5), 1267–1280.
Heaton, T. H. (1990), Evidence for and implications of self-healing pulses of slip in earthquake rupture, *Phys. Earth Planet. Inter.*, *64*(1), 1–20.
Huang, Y., and J.-P. Ampuero (2011), Pulse-like ruptures induced by low-velocity fault zones, *J. Geophys. Res.*, *116*, B12307, doi:10.1029/2011JB008684.
Huang, Y., D. V. Helmberger, and J.-P. Helmberger (2013), Rupture propagating at the forbidden speed: Is fault zone structure playing a role?, Abstract T53D-2608 presented at 2013 Fall Meeting, AGU, San Francisco, Calif., 9–13 Dec.
Johri, M., E. M. Dunham, M. D. Zoback, and Z. Fang (2014), Prediction fault damage zone by modeling dynamic rupture propagation and comparison with field observations, *J. Geophys. Res. Solid Earth*, doi:10.1002/2013JB010335.
Kaneko, Y., N. Lapusta, and J.-P. Ampuero (2008), Spectral-element modeling of spontaneous earthquake rupture on rate and state faults: Effect of velocity-strengthening friction at shallow depths, *J. Geophys. Res.*, *113*(B9), B09317, doi:10.1029/2007JB005553.
Kaneko, Y., J.-P. Ampuero and N. Lapusta (2011), Spectral-element simulations of long-term fault slip: Effect of low-rigidity layers on earthquake-cycle dynamics, *J. Geophys. Res.*, *116*, B10313, doi:10.1029/2011JB008395.
Komatitsch, D., and J. Tromp (1999), Introduction to the spectral element method for three-dimensional seismic wave propagation, *Geophys. J. Int.*, *139*(3), 806–822, doi:10.1046/j.1365-246X.1999.00967.x.
Lewis, M. A., and Y. Ben-Zion (2010), Diversity of fault zone damage and trapping structures in the Parkfield section of the San Andreas Fault from comprehensive analysis of near fault seismograms, *Geophys. J. Int.*, *183*(3), 1579–1595, doi:10.1111/j.1365-246X.2010.04816.x.
Lewis, M. A., Z. Peng, Y. Ben-Zion, and F. L. Vernon (2005), Shallow seismic trapping structure in the San Jacinto fault zone near Anza, California, *Geophys. J. Int.*, *162*(3), 867–881, doi:10.1111/j.1365-246X.2005.02684.x.
Li, Y.-G., J. E. Vidale, S. M. Day, D. D. Oglesby, and the SCEC Field Working Team (2002), Study of the 1999 M 7.1 Hector Mine, California, earthquake fault plane by trapped waves, *Bull. Seismol. Soc. Am.*, *92*(4), 1318–1332.

Li, Y. G., P. Chen, E. S. Cochran, J. E. Vidale, and T. Burdette (2006), Seismic evidence for rock damage and healing on the San Andreas fault associated with the 2004 M 6.0 Parkfield earthquake, *Bull. Seismol. Soc. Am.*, *96*(4B), S349–S363, doi:10.1785/0120050803.
Li, H., L. Zhu, and H. Yang (2007), High-resolution structures of the Landers fault zone inferred from aftershock waveform data, *Geophys. J. Int.*, *171*(3), 1295–1307, doi:10.1111/j.1365-246X.2007.03608.x.
Luo, Y., Y. Tan, S. Wei, D. Helmberger, Z. Zhan, S. Ni, E. Hauksson, and Y. Chen (2010), Source mechanism and rupture directivity of the 18 May 2009 Mw 4.6 Inglewood, California, Earthquake, *Bull. Seismol. Soc. Am.*, *100*(6), 3269–3277, doi:10.1785/0120100087.
Madariaga, R. (1976), Dynamics of an expanding circular fault, *Bull. Seismol. Soc. Am.*, *66*(3), 639–666.
Madariaga, R., J.-P. Ampuero, and M. Adda-Bedia (2006), Seismic radiation from simple models of earthquakes, in *Radiation Energy and the Physics of Earthquakes*, *AGU Monograph*, edited by A. McGarr et al., pp. 223–236, AGU, Washington D. C.
Mizuno, T., Y. Kuwahara, H. Ito, and K. Nishigami (2008), Spatial variations in fault-zone structure along the Nojima fault, central Japan, as inferred from borehole observations of fault-zone trapped waves, *Bull. Seismol. Soc. Am.*, *98*(2), 558–570, doi:10.1785/0120060247.
Moczo, P., J. Kristek, and L. Halada (2004), *The Finite-Difference Method for Seismologists. An Introduction*, pp. 158, Comenius Univ., Bratislava.
Pelties, C., Y. Huang, and J.-P. Ampuero (2013), Pulse-like rupture induced by three-dimensional fault zone flower structures, Abstract EGU2013-269 presented at EGU General Assembly 2013, EGU, Vienna, Austria, 7–12 Apr.
Peng, Z., Y. Ben-Zion, A. J. Michael, and L. Zhu (2003), Quantitative analysis of seismic fault zone waves in the rupture zone of the 1992 Landers, California, earthquake: Evidence for a shallow trapping structure, *Geophys. J. Int.*, *155*(3), 1021–1041, doi:10.1111/j.1365-246X.2003.02109.x.
Perrin, G., J. R. Rice, and G. Zheng (1995), Self-healing slip pulse on a frictional surface, *J. Mech. Phys. Solids*, *43*(9), 1461–1495.
Reches, Z., and D. A. Lockner (2010), Fault weakening and earthquake instability by powder lubrication, *Nature*, *467*, 452–455, doi:10.1038/nature09348.
Rempe, M. T., J. Mitchell, S. Renner, Y. B.-Z. Nippress, and T. Rockwell (2013), Damage and seismic velocity structure of pulverized rocks near the San Andreas Fault, *J. Geophys. Res. Solid Earth*, *118*, 2813–2831, doi:10.1002/jgrb.50184.
Rice, J. R. (1993), Spatio-temporal complexity of slip on a fault, *J. Geophys. Res.*, *98*, 9885–9907, doi:10.1029/93JB00191.
Rice, J. R. (2006), Heating and weakening of faults during earthquake slip, *J. Geophys. Res.*, *111*, B05311, doi:10.1029/2005JB004006.
Rice, J. R., C. G. Sammis, and R. Parsons (2005), Off-fault secondary failure induced by a dynamic slip pulse, *Bull. Seismol. Soc. Am.*, *95*(1), 109–134, doi:10.1785/0120030166.
Rowe, C. D., J. C. Moore, F. Remitti, and the IODP Expedition 343/343T Scientists (2013), The thickness of subduction plate boundary faults from the seafloor into the seismogenic zone, *Geology*, *41*(9), 991–994, doi:10.1130/G34556.1.
Sagy, A., and D. Korngreen (2012), Dynamic branched fractures in pulverized rocks from a deep borehole, *Geology*, *40*(9), 799–802, doi:10.1130/G33194.1.
Savage, H. M., and E. E. Brodsky (2011), Collateral damage: Evolution with displacement of fracture distribution and secondary fault strands in fault damage zones, *J. Geophys. Res.*, *116*, B03405, doi:10.1029/2010JB007665.
Scholz, C. H. (1987), Wear and gouge formation in brittle faulting, *Geology*, *15*(6), 493–495, doi:10.1130/0091-7613(1987)15<493:WAGFIB>2.0.CO;2.
Shaw, B. E., and J. R. Rice (2000), Existence of continuum complexity in the elastodynamics of repeated fault ruptures, *J. Geophys. Res.*, *105*(B10), 23,791–23,810, doi:10.1029/2000JB900203.
Sibson, R. H. (1986), Brecciation processes in fault zones: Inferences from earthquake rupturing, *Pure Appl. Geophys.*, *124*(1–2), 159–175, doi:10.1007/BF00875724.
Smith, D. E., and T. H. Heaton (2011), Models of stochastic, spatially varying stress in the crust compatible with focal-mechanism data, and how stress inversions can be biased toward the stress rate, *Bull. Seismol. Soc. Am.*, *101*(3), 1396–1421, doi:10.1785/0120100058.
Spudich, P., and E. Cranswick (1984), Direct observation of rupture propagation during the 1979 Imperial Valley earthquake using a short baseline accelerometer array, *Bull. Seismol. Soc. Am.*, *74*(6), 2083–2114.
Tan, Y., and D. Helmberger (2010), Rupture directivity characteristics of the 2003 Big Bear Sequence, *Bull. Seismol. Soc. Am.*, *100*(3), 1089–1106, doi:10.1785/0120090074.
Templeton, E. L., and J. R. Rice (2008), Off-fault plasticity and earthquake rupture dynamics: 1. Dry materials or neglect of fluid pressure changes, *J. Geophys. Res.*, *113*, B09306, doi:10.1029/2007JB005529.
Walker, K. T., and P. M. Shearer (2009), Illuminating the near-sonic rupture velocities of the intracontinental Kokoxili Mw 7.8 and Denali fault Mw 7.9 strike-slip earthquakes with global P wave back projection imaging, *J. Geophys. Res.*, *114*, B02304, doi:10.1029/2008JB005738.
Weertman, J. (1980), Unstable slippage across a fault that separates elastic media of different elastic constants, *J. Geophys. Res.*, *85*(B3), 1455–1461, doi:10.1029/JB085iB03p01455.
Weertman, J. (2014), Transonic gliding edge dislocations/slip pulse near and on an interface/fault, *J. Geophys. Res. Solid Earth*, *119*, 530–548, doi:10.1002/2013JB010121.
Xia, K., A. J. Rosakis, and H. Kanamori (2004), Laboratory earthquakes: The sub-Rayleigh-to-supershear rupture transition, *Science*, *303*(5665), 1859–1861, doi:10.1126/science.1094022.
Xu, S., J. P. Ampuero, Y. Ben-Zion, and V. Lyakhovsky (2009), Dynamic rupture on a frictional interface with off-fault damage, *Eos Trans. AGU*, *90*(52), Fall Meet. Suppl., Abstract T43A-2040.
Xu, S., Y. Ben-Zion, and J.-P. Ampuero (2012), Properties of inelastic yielding zones generated by in-plane dynamic ruptures-I. Model description and basic results, *Geophys. J. Int.*, *191*(3), 1325–1342, doi:10.1111/j.1365-246X.2012.05679.x.
Yang, H., and L. Zhu (2010), Shallow low-velocity zone of the San Jacinto fault from local earthquake waveform modeling, *Geophys. J. Int.*, *183*(1), 421–432, doi:10.1111/j.1365-246X.2010.04744.x.
Yang, H., L. Zhu, and E. S. Cochran (2011), Seismic structures of the Calico fault zone inferred from local earthquake travel time modeling, *Geophys. J. Int.*, *186*(2), 760–770, doi:10.1111/j.1365-246X.2011.05055.x.
Zheng, G., and J. R. Rice (1998), Conditions under which velocity-weakening friction allows a self-healing versus a cracklike mode of rupture, *Bull. Seismol. Soc. Am.*, *88*(6), 1466–1483.